

Pseudoscalar Higgs Boson Decays into W and Z Bosons Revisited

Werner Bernreuther¹, Patrick González², Martin Wiebusch³

Institut für Theoretische Physik, RWTH Aachen University, 52056 Aachen, Germany

Abstract

We examine, in a number of Standard Model extensions, whether the decays $A \rightarrow WW/ZZ$ of a neutral pseudoscalar (Higgs) resonance can have branching ratios at the percent level and we determine the possible size of $B(A \rightarrow WW/ZZ)$ relative to the respective branching ratios of a scalar boson H . The branching ratios of these decay modes and the total widths Γ_A, Γ_H are computed in the minimal supersymmetric extension of the SM, in a type-II two-Higgs doublet extension (2HDM), in a 2HDM with 4 chiral fermion generations, in a 2HDM with additional heavy vector-like quarks, and in a top-color assisted technicolor model. We find that in the above non-supersymmetric models $B(A \rightarrow WW)$ can be about 2%, while $B(A \rightarrow ZZ) \lesssim 10^{-3}$. The ratio $B(A \rightarrow WW)/B(H \rightarrow WW)$ can be of order 10% in large regions of the parameter space of the models.

PACS number(s): 12.60.-i, 12.60.Fr, 12.60Jv, 12.60.Nz, 14.80.Cp

Keywords: Higgs boson decay, weak gauge bosons, standard model extensions

¹Email: breuther@physik.rwth-aachen.de

²Email: gonzalez@physik.rwth-aachen.de

³Email: mwiebusch@physik.rwth-aachen.de

1 Introduction

The search for Higgs bosons or, more general, (spin-zero) resonances is among the major physics goals of present-day collider physics, as the existence of such resonances and exploration of their properties (quantum numbers, production and decay modes) would yield decisive clues for unraveling the mechanism of electroweak gauge symmetry breaking (EWSB). There is an exhaustive phenomenology of the production and decay modes of the standard model (SM) Higgs boson; likewise, there are extensive theoretical studies of these issues for spin-zero (Higgs) particles predicted by popular SM extensions. (For reviews see, e.g., [1] and [2, 3, 4], respectively.)

For the SM Higgs boson H with a mass $m_H \gtrsim 130$ GeV, signatures from the decay modes⁴ $H \rightarrow WW^{(*)}/ZZ^{(*)}$ have the highest discovery potential for this particle at the Large Hadron Collider (LHC) [6, 7]. Concerning non-standard neutral Higgs particles the situation is, especially in view of unknown model parameters, less clear as to which decay channel is, for a specific production mode, the most promising one. However, as is well-known, for a pseudoscalar Higgs boson A it is expected that the decays $A \rightarrow WW/ZZ$ are strongly suppressed. This is because the couplings AVV ($V = W, Z$) must be loop-induced, and they turn out to be very small in two-Higgs doublet extensions (2HDM) and the minimal supersymmetric extension (MSSM) of the SM [8, 9]. In view of this conventional wisdom one might be inclined to conclude that the discovery of a spin-zero resonance in the WW and/or ZZ channel immediately suggests that this resonance is a scalar, i.e., a $J^{PC} = 0^{++}$ state. We hasten to add that many suggestions and phenomenological studies have been made how the spin and the CP parity of a resonance can actually be measured in these channels [3, 10, 11, 12, 13, 14, 15, 16, 17].

In this paper, we examine whether the decays of a neutral pseudoscalar into WW/ZZ can have branching ratios at the percent level and analyse the possible size of $B(A \rightarrow WW/ZZ)$ relative to the respective branching ratios of a scalar boson H . We analyze this in the context of several phenomenologically viable SM extensions. Concerning the scenario that EWSB is triggered by elementary Higgs fields, we choose a Higgs sector which is composed of two SU(2) doublets. For the convenience of the reader we first reexamine $B(A \rightarrow VV)$ in 2HDM and the MSSM. Our analysis for models with additional heavy (exotic) quarks and leptons is new, to the best of our knowledge. We choose top-color assisted technicolor models (TC2) [18] as a paradigm for models that predict a relatively light composite pseudoscalar.

We assume here that the dynamics of the EWSB sector of the Yukawa interactions is such that the electrically neutral Higgs resonances are CP eigenstates in the mass basis, at least to very good approximation. If the Higgs sector violates CP then, as is well known, the neutral spin-zero mass eigenstates are, in general, a mixture of a CP-odd and CP-even component, of which the latter has tree-level couplings to WW/ZZ .

⁴For state-of-the-art predictions for $H \rightarrow WW/ZZ \rightarrow 4$ fermions, see [5].

The paper is organized as follows. In Sect. 2, we compute for the above models the branching ratios $B(A \rightarrow VV)$ for masses $m_A \geq 200$ GeV. We estimate the maximal size of these branching ratios and the total width Γ_A within a given model. For comparison we also determine the branching ratios $H \rightarrow VV$ of a scalar H with mass $m_H \simeq m_A$ and its width Γ_H . We conclude in Sect. 3. In an appendix we list for the convenience of the reader, for our model with vector-like quarks, the couplings of these quarks to Higgs bosons.

2 Models and results

First, we collect a few basic formulae needed in the next section. Lorentz covariance dictates that the amplitude for the decay of a spin-zero state ϕ into a pair of vector bosons, $\phi(p) \rightarrow V(p_1)V(p_2)$ ($V = W, Z$) contains in general three form factors:

$$i\mathcal{M}_{VV} = f_{1,VV} \varepsilon_1^* \cdot \varepsilon_2^* + f_{2,VV} (p_1 \cdot \varepsilon_2^*)(p_2 \cdot \varepsilon_1^*) + f_{3,VV} \varepsilon_{\mu\nu\rho\sigma} p_1^\mu p_2^\nu \varepsilon_1^{*\rho} \varepsilon_2^{*\sigma} \quad , \quad (1)$$

where ε_1 and ε_2 are the polarization vectors of the vector bosons. For a pseudoscalar, $\phi = A$, the form factors $f_{1,VV}$ and $f_{2,VV}$ vanish if CP is conserved. Defining for this case the effective dimensionless coupling C_{VV} by

$$f_{3,VV} \equiv \frac{e}{s_W m_W} C_{VV} \quad , \quad (2)$$

where s_W (c_W) denotes the sine (cosine) of the weak mixing angle, one obtains for the decay rate of a pseudoscalar into a pair of on-shell vector bosons:

$$\Gamma(A \rightarrow VV) = r_V \frac{G_F}{8\sqrt{2}\pi} m_A^3 \beta_V^3 |C_{VV}|^2 \quad , \quad (3)$$

where $\beta_V = (1 - 4m_V^2/m_A^2)^{\frac{1}{2}}$ and $r_V = 2$ (1) for $V = W$ (Z).

In gauge theories, or more general in renormalizable theories, the coupling $f_{3,VV}$ is not present at tree level, but must be induced by loop corrections. In the bosonic sectors of the SM extensions considered in the next section, C and P are separately conserved. Thus, the bosonic sectors of these theories cannot induce, at any order, a non-zero AVV coupling – it requires fermions which, through their C- and P-violating couplings to W and Z bosons, generate $f_{3,VV} \neq 0$ at 1-loop order. If the Yukawa couplings of A are of the Higgs-boson type, then C_{VV} exhibits the well-known non-decoupling behaviour of Higgs boson interactions. In this case, C_{VV} does not vanish for heavy fermion(s) circulating in the loop, but becomes independent of the internal mass(es).

For completeness we also list the rates of the decays of a scalar (Higgs) boson H into a WW and ZZ , as we will compare the $A, H \rightarrow VV$ branching ratios in the next section. The HVV amplitude at Born level can be parameterized by $2m_V^2 \sqrt{\sqrt{2}G_F} h_{VV} \varepsilon_1^* \cdot \varepsilon_2^*$,

where h_{VV} is a dimensionless coupling which is equal to one in the SM. The tree-level decay rate is

$$\Gamma(H \rightarrow VV) = r_V \frac{G_F}{16\sqrt{2}\pi} m_H^3 \beta_V \left[\beta_V^2 + 12 \frac{m_V^4}{m_H^4} \right] h_{VV}^2 \quad . \quad (4)$$

Below we shall discuss SM extensions with two SU(2) Higgs doublets as a paradigm for an extended Higgs sector, with a dynamics such that the physical spin-zero mass eigenstates are also CP eigenstates. That is, the Higgs boson spectrum contains, apart from a charged Higgs-boson pair H^\pm , two CP-even states h, H and a CP-odd state A . The mass of A is assumed to be $m_A \geq 200$ GeV. For comparison, we consider also the decay of the heavier of the two CP-even Higgs bosons, denoted by H , into W^+W^- and ZZ . We define the ratios

$$R_V = \frac{B(A \rightarrow VV)}{B(H \rightarrow VV)} \quad , \quad (5)$$

for comparing the respective branching ratios of A and H .

We will also consider top-color assisted technicolor, which is a phenomenologically viable model for “dynamical” gauge symmetry breaking. The spin-zero particle spectra of this class of models contain a triplet of “top pions”, $\Pi^{0,\pm}$, of which Π^0 takes the role of the pseudoscalar A , and a scalar bound state, the “top Higgs” H_t , with a mass of the order of a few hundred GeV.

Throughout this paper we will use the following SM parameters:

$$\begin{aligned} 1/\alpha_{\text{em}} &= 137.036 \quad , \quad \alpha_s = 0.118 \quad , \\ m_Z &= 91.19 \text{ GeV} \quad , \quad m_W = 80.40 \text{ GeV} \quad , \\ m_t &= 172.6 \text{ GeV} \quad , \quad m_b = 4.79 \text{ GeV} \quad , \quad m_\tau = 1.78 \text{ GeV} \quad , \quad V_{tb} = 1 \quad . \end{aligned} \quad (6)$$

In view of the small Yukawa couplings of the quarks and leptons of the first and second generation, their interactions with the Higgs resonances can be neglected in the analysis below. For the calculations we used `FeynArts` [19, 20] in combination with `FormCalc` and `LoopTools` [21, 22].

2.1 Two-Higgs doublet extensions

We consider here a type-II two-Higgs doublet extension (2HDM) [23] of the SM (with CP-invariant tree-level Higgs potential), where by construction flavour-changing neutral current interactions are absent at tree level. The Higgs sector of this model involves, besides the masses of the charged and the three neutral Higgs bosons, three more free parameters, which are commonly denoted as $\tan\beta$, α and λ_5 . The parameter $\tan\beta$ is the ratio v_u/v_d , where $v_{u,d}$ are the vacuum expectation values of the neutral components of the Higgs doublet fields $\Phi_{u,d}$. The angle α describes the mixing of the two CP-even

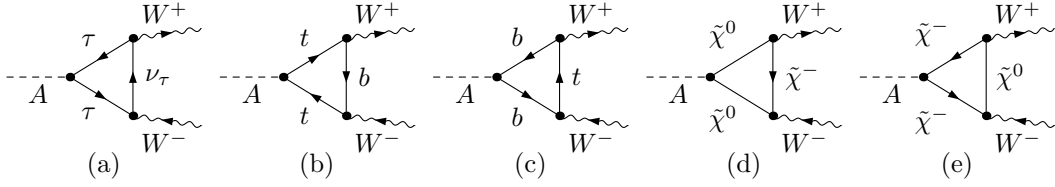


Figure 1: Diagrams that contribute in the MSSM to the decay $A \rightarrow WW$. In the 2HDM the 1-loop decay amplitude is due to the diagrams (a–c) only. As we consider decays to on-shell gauge bosons, diagrams involving the AZ transition amplitude are absent.

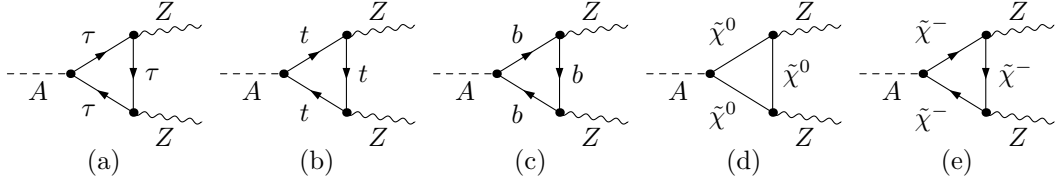


Figure 2: Diagrams that contribute in the MSSM to the decay $A \rightarrow ZZ$. In the case of charged particles in the loop the diagrams with reversed charge flow have been omitted. In the 2HDM the 1-loop decay amplitude is due to the diagrams (a–c) only.

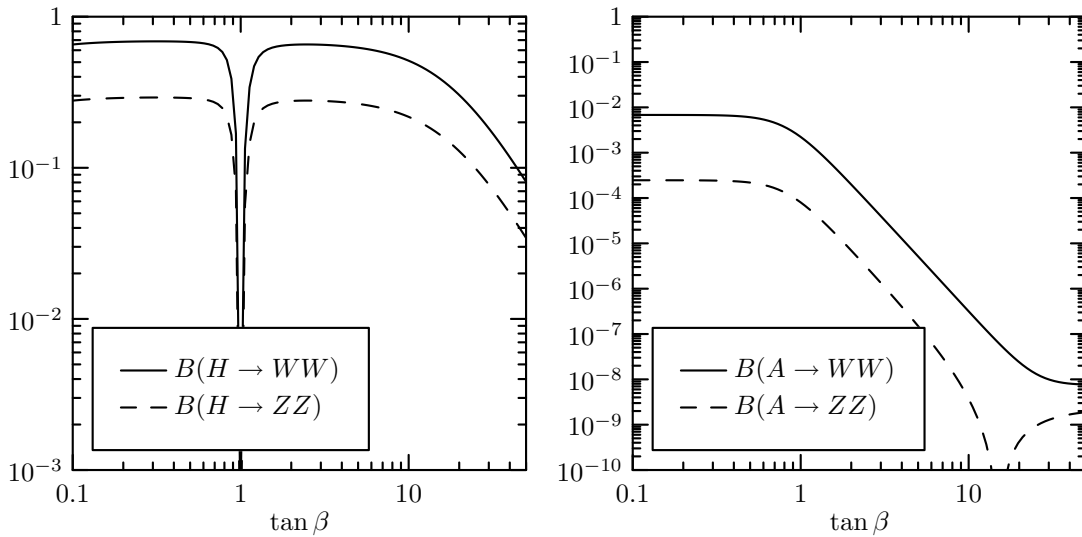


Figure 3: The branching ratios for $H \rightarrow WW, ZZ$ (left) and $A \rightarrow WW, ZZ$ (right) in the 2HDM as functions of $\tan \beta$ for $m_H = m_A = 250$ GeV, $m_h = 160$ GeV, and $\alpha = -\pi/4$.

neutral Higgs states which leads to the mass eigenstates h and H . The parameter λ_5 is a dimensionless coupling from the term

$$\lambda_5(\frac{1}{2}(\Phi_d^\dagger\Phi_u + \Phi_u^\dagger\Phi_d) - v_u v_d)^2 \quad (7)$$

in the Higgs potential.⁵

The decays $A \rightarrow WW$ and $A \rightarrow ZZ$ are mediated by the 1-loop diagrams (a-c) of Fig. 1 and Fig. 2, respectively. For computing the branching ratios $B(A, H \rightarrow WW/ZZ)$, we need to determine the total widths of A and H . For this purpose the following decays should in addition be taken into account, if kinematically possible:

$$\begin{aligned} H &\rightarrow W^\pm H^\mp, hh, b\bar{b}, \tau\bar{\tau}, t\bar{t}, gg, \\ A &\rightarrow W^\pm H^\mp, Zh, b\bar{b}, \tau\bar{\tau}, t\bar{t}, gg \quad . \end{aligned} \quad (8)$$

Apart from the gg mode, these decays are induced already at tree level. The $H, A \rightarrow gg$ decay amplitudes are given by diagrams analogous to Fig. 2 (b,c) and are dominated by the top-quark loop for small and moderate values of $\tan\beta$. For definiteness we put the mass of the light scalar Higgs boson

$$m_h = 160 \text{ GeV} . \quad (9)$$

As our goal is to investigate how large the branching ratios $B(A \rightarrow WW/ZZ)$ and the ratios R_W, R_Z defined in (5) can become, we choose the mass of H^\pm such that the decays $A \rightarrow W^\pm H^\mp$ are kinematically forbidden. (In fact, a charged Higgs boson with a mass below 315 GeV is excluded in the 2HDM on empirical grounds [24].)

First we consider a relatively light pseudoscalar A and, for comparison, a scalar H of the same mass: $m_A = m_H = 250$ GeV. Then, apart from $A, H \rightarrow W^\pm H^\mp$, also the channels $A \rightarrow Zh, t\bar{t}$ and $H \rightarrow hh, t\bar{t}$ are closed in view of the chosen Higgs-boson masses. The resulting branching ratios for $H, A \rightarrow WW/ZZ$ are shown as functions of $\tan\beta$ in Fig. 3, for a fixed mixing angle $\alpha = -\pi/4$. For small $\tan\beta$ the total H decay width is dominated by the decays $H \rightarrow WW, ZZ$. (The gg mode contributes about 6% for $\tan\beta = 0.1$.) As the Born amplitudes of both modes are proportional to $\cos(\beta - \alpha)$ the branching ratios $B(H \rightarrow VV)$ are almost constant in that region. For $|\beta - \alpha| = \pi/2$, i.e., $\tan\beta = 1$ for our choice of α , the Born amplitudes vanish, which causes the sharp dip in Fig. 3 (left panel). The one-loop corrections render the amplitude non-zero, and we expect $B(H \rightarrow VV) \approx B(A \rightarrow VV)$ in that region of parameter space. For large $\tan\beta$ the width of $H \rightarrow b\bar{b}$ gets bigger and eventually exceeds those of $H \rightarrow VV$. As a result the $H \rightarrow WW, ZZ$ branching ratios decrease for large $\tan\beta$.

The total A decay width is dominated, for small $\tan\beta$, by the contribution from $A \rightarrow gg$. The $A \rightarrow WW, ZZ, gg$ decay amplitudes are essentially determined by the diagrams where A couples to the top quark, i.e., they are all proportional to $\cot\beta$.

⁵See [23] for details.

Thus the branching ratios of $A \rightarrow WW, ZZ$ are approximately constant for $\tan \beta \lesssim 1$. For $\tan \beta > 1$ the $A \rightarrow WW, ZZ, gg$ partial widths get smaller with increasing $\tan \beta$ and the (tree-level) $A \rightarrow b\bar{b}$ partial width, which is proportional to $\tan^2 \beta$, begins to dominate. As a result the branching ratios $B(A \rightarrow WW, ZZ)$ decrease for $\tan \beta > 1$ in the range shown in Fig. 3.

In Fig. 4 the branching ratios of $H, A \rightarrow WW/ZZ$ are shown as functions of $m_{H,A}$ for three different values of $\tan \beta$. In order to exclude the region around $|\beta - \alpha| = \pi/2$ we put $\alpha = \beta - \pi/4$. The mass of h is again chosen to be $m_h = 160$ GeV. Fig. 4 shows that, once the decay channel $H \rightarrow hh$ is open, the branching ratios $B(H \rightarrow VV)$ decrease significantly if $\tan \beta$ is markedly smaller or larger than one, because in a generic 2HDM the $H \rightarrow hh$ amplitude is proportional to $1/\sin 2\beta$, so that $H \rightarrow hh$ dominates the total width Γ_H , if $\tan \beta$ is small or large. Note, however, that the Hhh vertex also contains a term proportional to λ_5 . Here we set

$$\lambda_5 = 0 \quad , \quad (10)$$

but it is also possible to tune λ_5 to cancel the enhancement factor $1/\sin 2\beta$. In fact, this is precisely what happens in the MSSM, where λ_5 is no longer an independent parameter.

As far as A is concerned, the opening of $A \rightarrow Zh$ (the amplitude of which is proportional to $\cos(\beta - \alpha)$) has a less dramatic effect on the $A \rightarrow VV$ branching ratios. Once $A \rightarrow t\bar{t}$ is kinematically possible, they drop, however, significantly if $\tan \beta$ is not very large.

For completeness we show in Fig. 5 the total widths of A and H as functions of m_ϕ ($\phi = H, A$) for $\tan \beta = 0.2$, $\alpha = \beta - \pi/4$ and $m_h = 160$ GeV. We see that the H total width increases rapidly when the $H \rightarrow hh$ channel opens. As pointed out above, this is due to the $1/\sin 2\beta$ enhancement of the Hhh vertex. The total width of A increases even more dramatically when the $A \rightarrow t\bar{t}$ channel opens. This only happens for small values of $\tan \beta$, where the $At\bar{t}$ coupling is enhanced. In fact, for large $\tan \beta$ and $m_A > 2m_t$ the width Γ_A very quickly gets as large as m_A so that the pseudoscalar Higgs would no longer be visible as a resonance.

We conclude that in the 2HDM the branching ratios $B(A \rightarrow WW) \lesssim 10^{-2}$ and $B(A \rightarrow ZZ) \lesssim 10^{-3}$. In the case of the WW final state the percent level can be reached if $m_A \leq 2m_t$. The corresponding branching ratios of the heavy scalar Higgs boson H with a mass $2m_V < m_H < 2m_t$ can be quite small, $B(H \rightarrow WW) \gtrsim 6 \times 10^{-2}$ and $B(H \rightarrow ZZ) \gtrsim 3 \times 10^{-2}$, if $\tan \beta$ is significantly smaller or larger than one and $H \rightarrow hh$ is kinematically possible and enhanced. Then this mode dominates the total width Γ_H , which gets rather large. In this case and for parameters as in Fig. 4 the ratios (5) are $R_W \lesssim 0.17$ and $R_Z < 0.03$. However, in a small region of parameter space, in the close vicinity of $|\beta - \alpha| = \pi/2$, these ratios can be even of order one.

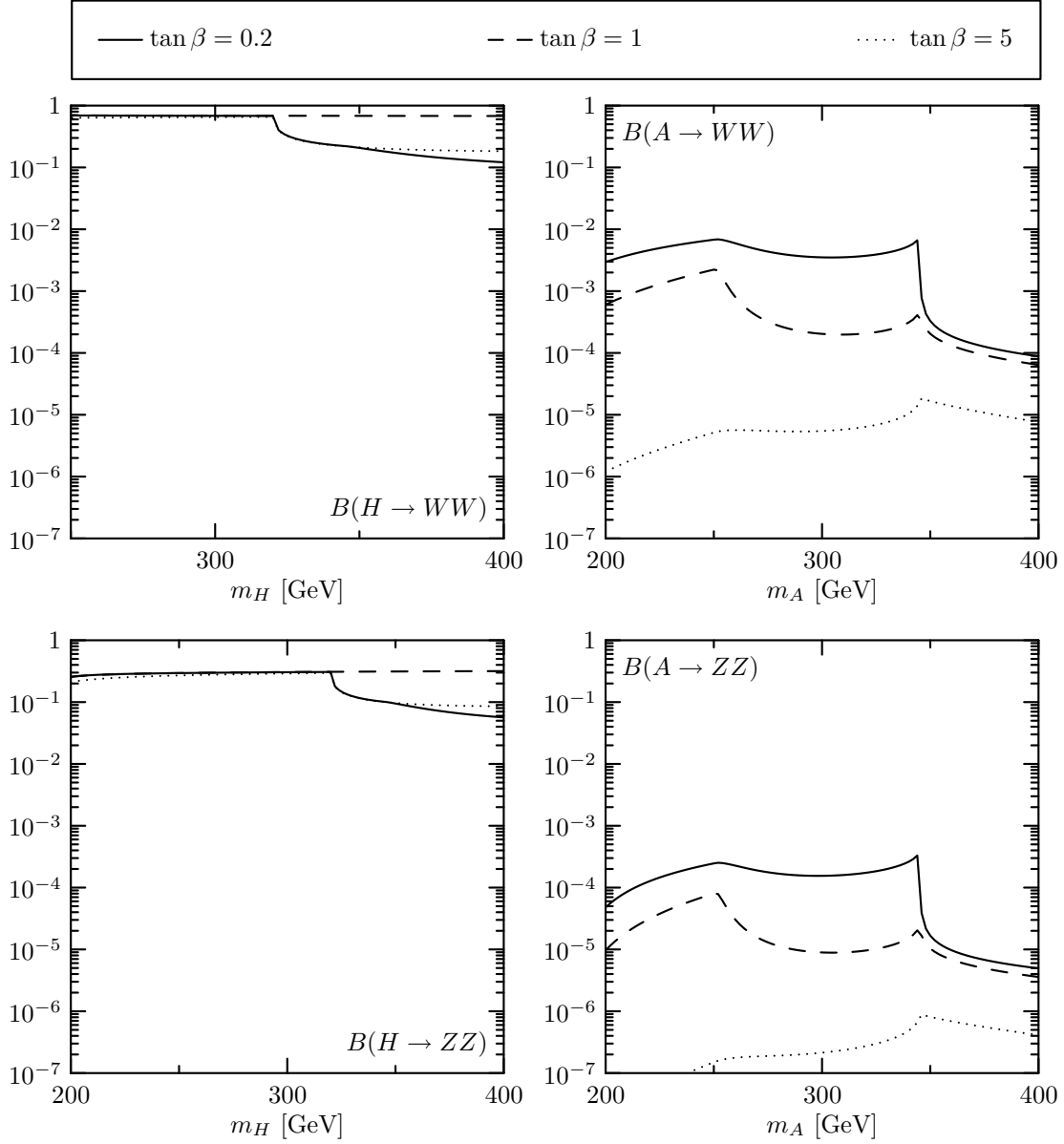


Figure 4: The branching ratios for $H \rightarrow WW, ZZ$ (left) and $A \rightarrow WW, ZZ$ (right) in the 2HDM as functions of m_H and m_A , respectively, for three different values of $\tan \beta$. The mixing angle α is chosen such that $\alpha = \beta - \pi/4$, and $m_h = 160$ GeV.

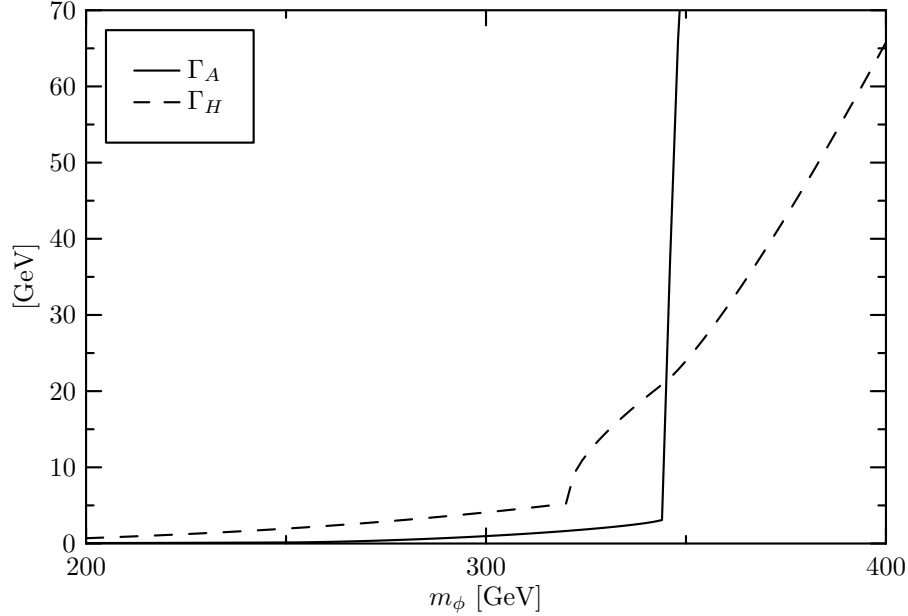


Figure 5: The total widths of H and A in the 2HDM as functions of m_ϕ ($\phi = H, A$) for $\tan\beta = 0.2$, $\alpha = \beta - \pi/4$ and $m_h = 160$ GeV.

2.2 The MSSM

In the MSSM the masses of the neutral Higgs bosons and the mixing angle α are no longer independent parameters. At tree level they can be expressed in terms of the charged Higgs-boson mass m_{H^\pm} and $\tan\beta$ as follows:

$$m_A^2 = m_{H^\pm}^2 + m_W^2 \quad , \quad (11a)$$

$$m_{H,h}^2 = \frac{1}{2} \left[m_A^2 + m_Z^2 \pm \sqrt{(m_A^2 + m_Z^2)^2 - 4m_Z^2 m_A^2 \cos^2 2\beta} \right] \quad , \quad (11b)$$

$$\cos(2\alpha) = -\cos(2\beta) \frac{m_A^2 - m_Z^2}{m_H^2 - m_h^2} \quad , \quad \sin(2\alpha) = -\sin(2\beta) \frac{m_H^2 + m_h^2}{m_H^2 - m_h^2} \quad . \quad (11c)$$

For MSSM scenarios with $m_{H^\pm} \gg m_Z$ these equations yield

$$m_A \approx m_H \quad , \quad \beta - \alpha \approx \frac{\pi}{2} \quad . \quad (12)$$

The HWW and HZZ Born vertices are proportional to $\cos(\beta - \alpha)$, as in the 2HDM. Consequently the $H \rightarrow WW$ and $H \rightarrow ZZ$ branching ratios are naturally suppressed in MSSM scenarios with heavy Higgs particles.

However, it is well known that the tree-level relations (11) are substantially modified by loop corrections to the MSSM Higgs potential. These corrections are responsible for pushing the the mass of the light Higgs boson above the current lower limit of ≈ 115 GeV

and have to be taken into account to obtain reliable results. The lower limit on m_h implies that $\tan\beta \gtrsim 3$ in the MSSM.

Here we used `FeynHiggs` version 2.6.5 [25, 26, 27, 28] to calculate all one-loop and leading two-loop corrections to the neutral Higgs-boson self-energies in the MSSM and extract from them the physical neutral Higgs masses, LSZ residues, and the resulting effective mixing angle α . Our results for the partial widths of H and A were then calculated with these effective parameters. It turns out that the approximations (12) for m_{H^\pm} being large are still valid if loop corrections to the Higgs potential are taken into account. Consequently the factor $\cos(\beta - \alpha)$ in the HVV vertices is still small. Our SUSY parameters are chosen in such a way that the following mass bounds are satisfied:

$$m_h \gtrsim 115 \text{ GeV} \quad , \quad m_{\chi_1^+} \gtrsim 100 \text{ GeV} \quad , \quad m_{\chi_1^0} \gtrsim 50 \text{ GeV} \quad , \quad m_{\tilde{t}_1} \gtrsim 100 \text{ GeV} \quad , \\ m_{\tilde{t}_2}, m_{\tilde{q}}, m_{\tilde{l}}, m_{\tilde{\nu}} \gtrsim 500 \text{ GeV} \quad . \quad (13)$$

For this purpose, we fix the following soft masses and trilinear couplings:

$$\mu = 200 \text{ GeV} \quad , \quad M_1 = \frac{5}{3} \tan^2 \theta_W M_2 \quad , \quad m_{\tilde{g}} = 500 \text{ GeV} \quad , \\ M_{L_i} = M_{E_i} = M_{Q_i} = M_{D_i} = M_{U_{1,2}} = A_{L_i} = A_{U_{1,2}} = A_{D_i} = 500 \text{ GeV} \quad . \quad (14)$$

Here μ , M_1 , and M_2 are the soft SUSY breaking masses of the Higgs potential, M_L and M_E are the soft masses of the left- and right-handed sleptons, M_Q the soft masses of the left-handed squarks, and M_U and M_D the soft masses of the right-handed up- and down-type squarks. Likewise, A_L , A_U and A_D are the trilinear couplings of the sleptons, up-type squarks and down-type squarks, respectively. Furthermore $m_{\tilde{g}}$ is the gluino mass and $i = 1, 2, 3$ is a generation index. The relation between M_1 and M_2 is the usual GUT relation. Note that the $A \rightarrow VV$ partial widths are affected directly only by the parameters $\tan\beta$, μ , M_1 , and M_2 , because the only non-SM particles appearing in the loop diagrams in Fig. 1 and 2 are the charginos and neutralinos.

We left m_{H^\pm} , M_2 , M_{U_3} and A_{U_3} unspecified in (14). Rather than choosing values for these parameters directly, we will adjust them numerically to obtain specific values for the pseudoscalar mass m_A , the lightest Higgs-boson mass m_h , the lightest stop mass $m_{\tilde{t}_1}$, and the lightest neutralino mass $m_{\tilde{\chi}_1^0}$. Throughout this section we use

$$m_h = 115 \text{ GeV} \quad , \quad m_{\tilde{t}_1} = 400 \text{ GeV} \quad . \quad (15)$$

The MSSM diagrams that contribute to $A \rightarrow WW$ and $A \rightarrow ZZ$ decays are shown in figures 1 and 2, respectively. As we discussed in the 2HDM, the contributions from loops involving t or b quarks are rather small for $\tan\beta > 1$. As a result the dominant contributions to the $A \rightarrow WW, ZZ$ partial widths in the MSSM come from diagrams with charginos or neutralinos in the loop, as long as their masses are not substantially larger than m_A .

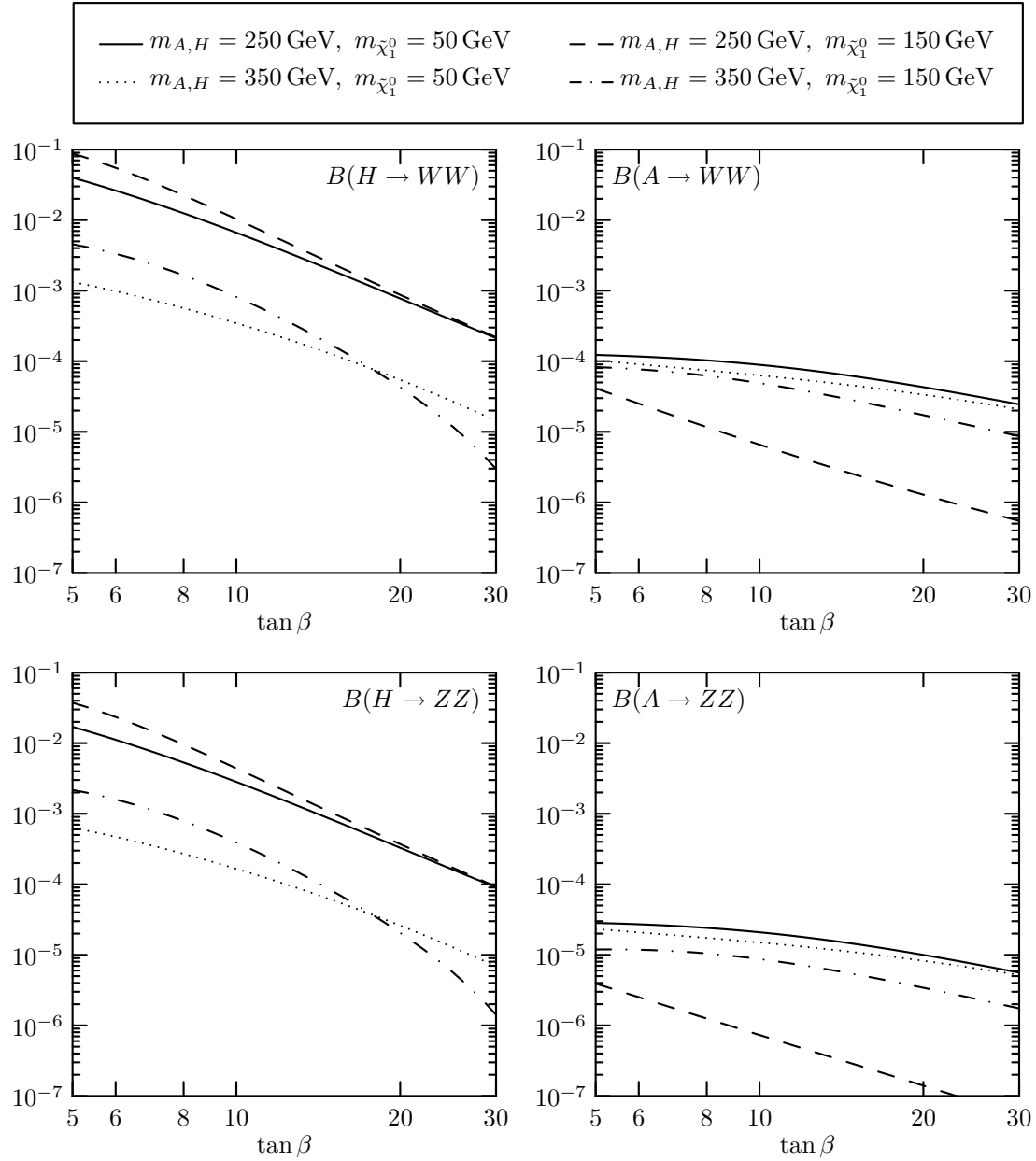


Figure 6: The MSSM branching ratios of the decays of H (left column) and A (right column) into WW (first row) and ZZ (second row) final states as functions of $\tan \beta$ for the parameters (6), (14), (15), and different combinations of m_A and $m_{\tilde{\chi}_1^0}$.

Fig. 6 shows the branching ratios of $H, A \rightarrow WW/ZZ$ as functions of $\tan\beta$ for the parameters (6), (14), (15) and for different combinations of m_A and $m_{\tilde{\chi}_1^0}$. The total widths of A and H were calculated with `FeynHiggs` [25, 26, 27, 28]. In our scenario the contributing decay channels are

$$\begin{aligned} H &\rightarrow b\bar{b}, \tau\bar{\tau}, t\bar{t}, gg, \chi_i^+ \chi_j^-, \chi_i^0 \chi_j^0, hh \quad , \\ A &\rightarrow b\bar{b}, \tau\bar{\tau}, t\bar{t}, gg, \chi_i^+ \chi_j^-, \chi_i^0 \chi_j^0, Zh \quad . \end{aligned} \quad (16)$$

For light $\tilde{\chi}_1^0$, $\tan\beta \gtrsim 5$, and $m_{H,A} < 2m_t$ the dominant contributions to the A and H total widths come from the decays into $b\bar{b}$, $\tilde{\chi}_1^+ \tilde{\chi}_1^-$ and $\tilde{\chi}_2^0 \tilde{\chi}_1^0$, provided the latter are kinematically allowed. For $\tan\beta \gtrsim 15$ the A and H total widths are dominated by the $b\bar{b}$ ($\sim 90\%$) and $\tau^-\tau^+$ ($\sim 10\%$) channels, as long as the $t\bar{t}$ channel is closed. In the $\tan\beta$ range shown in Fig. 6 the total widths of A and H grow by approximately one order of magnitude.

At the same time the $H \rightarrow WW, ZZ$ partial widths drop by approximately two orders of magnitude because $\cos(\beta - \alpha)$ becomes small. Nevertheless, for the parameters used in Fig. 6, the one-loop contributions to $H \rightarrow VV$ are still smaller than the Born terms. For large $\tan\beta$ and large $m_{A,H}$ the $H \rightarrow WW, ZZ$ branching ratios can actually be smaller than the corresponding A branching ratios.

The $A \rightarrow WW, ZZ$ partial widths and hence the $A \rightarrow WW, ZZ$ branching ratios are less sensitive to $\tan\beta$. However, $B(A \rightarrow WW) < 10^{-4}$ and $B(A \rightarrow ZZ) < 2 \times 10^{-5}$ for the parameters used in Fig. 6.

In Fig. 7 the branching ratios of $A \rightarrow WW, ZZ$ and $A \rightarrow ZZ$ are shown as functions of m_A for different values of $m_{\tilde{\chi}_1^0}$. The kinks correspond to the opening of decay channels into chargino or neutralino pairs. The drop in the branching ratio that is usually associated with the opening of a new channel is less pronounced here, because whenever the total width increases due to the opening of such a channel, a corresponding loop diagram from Fig. 1 or 2 develops an imaginary part, which leads to an increase in the $A \rightarrow WW, ZZ$ partial widths.

Fig. 8 shows the H and A total widths as functions of their mass for the parameters (6), (14), (15), $\tan\beta = 10$ and $m_{\tilde{\chi}_1^0} = 50$ GeV. The rapid increase of Γ_H at the opening of the $H \rightarrow hh$ threshold is absent here, because the MSSM constraints on the 2HDM Higgs potential parameters tune λ_5 in such a way that the enhancing factor $1/\sin 2\beta$ cancels in the Hhh coupling. Since $\tan\beta$ is large here, the opening of the $A \rightarrow t\bar{t}$ threshold also has no dramatic effect on the A total width. As a result, the A and H total widths stay below 6 GeV in the whole mass range $250 \text{ GeV} \leq m_\phi \leq 500 \text{ GeV}$.

From Figs. 6 and 7 we conclude that in the MSSM the decays $A \rightarrow WW, ZZ$ are really rare, as the branching ratios $B(A \rightarrow WW) \lesssim 10^{-4}$ and $B(A \rightarrow ZZ) \lesssim 2 \times 10^{-5}$. The branching ratios of the corresponding decays of the heavy scalar Higgs boson H depend sensitively on the MSSM parameters, in particular on the value of $\tan\beta$. In the scenario $m_{H^\pm}, m_H, m_A \gg m_Z$ the branching ratios $B(H \rightarrow WW, ZZ)$ are, for $m_H = 250$

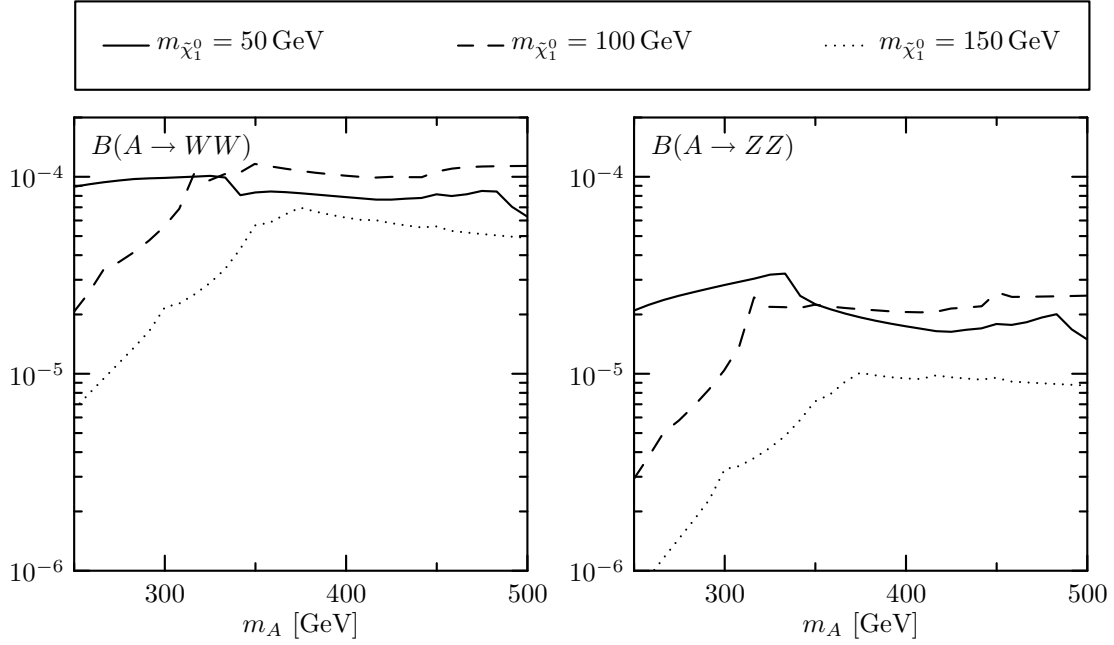


Figure 7: The branching ratios for $A \rightarrow WW$ (left) and $A \rightarrow ZZ$ (right) as functions of m_A for the parameters (6), (14), (15), $\tan \beta = 10$, and three different values of $m_{\tilde{\chi}_1^0}$.

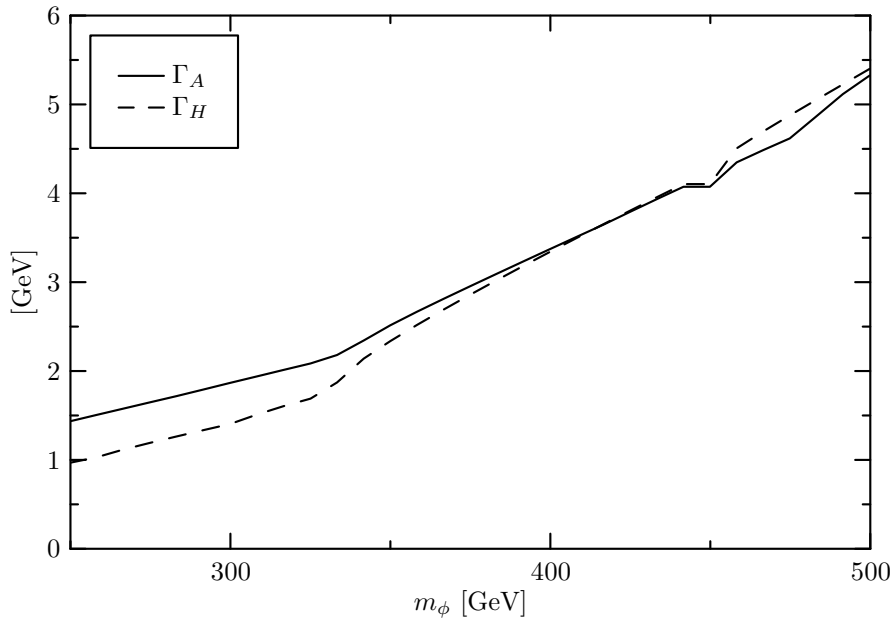


Figure 8: The H and A total widths in the MSSM as functions of m_ϕ ($\phi = H, A$) for the parameters (6), (14), (15), $\tan \beta = 10$ and $m_{\tilde{\chi}_1^0} = 50$ GeV.

GeV, about 0.09 and 0.04, respectively, for $\tan\beta = 5$, but drop below 10^{-3} for large $\tan\beta$.

2.3 A heavy fourth generation

Recently, there has been renewed interest in the question of whether a sequential fourth generation of chiral quarks and leptons (left-chiral doublets and right-chiral singlets) with masses in the (few) hundred GeV range can exist, in spite of strong experimental constraints (see, e.g., [29, 30]). In the following we shall denote the corresponding fourth generation quark and lepton mass eigenstates by u_4, d_4, ℓ_4, ν_4 . The strongest constraints on the masses of these states come from direct searches at LEP2 and at the Tevatron, and from electroweak precision observables. Non-observation at LEP2 implies the lower bounds $m_{\ell_4} > 100$ GeV, $m_{\nu_4} > 90$ GeV (for definiteness, we assume ν_4 to be a Dirac particle) [31], while searches for heavy quarks at the Tevatron yield the mass limits $m_{d_4} > 190$ GeV [31] and $m_{u_4} > 311$ GeV [32]. Strong constraints on a fourth generation are also implied by the oblique electroweak corrections, i.e., by the experimentally allowed values of the S, T and U parameters. While the mass splitting of the $I_W = \pm 1/2$ partners of a doublet need not be too large in order not to violate the bound on the ρ parameter respectively on T , degenerate doublets are not acceptable, too, because this would make the contribution δS to the S parameter too big. However, if $m_{u_4} > m_{d_4}$ and $m_{\ell_4} > m_{\nu_4}$ then $\delta S, \delta T$ can be brought in accord with the experimental constraints.

In the following we consider a type-II 2HDM as in Sect. 2.1 with four sequential quark and lepton generations. For our numerical analysis we use the following masses for the fourth generation fermions:

$$m_{d_4} = 200 \text{ GeV}, m_{u_4} = 320 \text{ GeV}, m_{\ell_4} = 220 \text{ GeV}, m_{\nu_4} = 180 \text{ GeV}. \quad (17)$$

As in Sect. 2.1 we put $m_h = 160$ GeV and $\beta - \alpha = \pi/4$.

Fig. 9 shows the H and A branching ratios into WW and ZZ as functions of the decaying particle's mass for different values of $\tan\beta$. The decays that contribute to the total widths are the same as in (8), because we keep $m_{H,A}$ below the production thresholds for the 4th generation fermions.

In order to discuss the contribution ΔC_{VV} of the fourth generation fermions to the amplitude C_{VV} of the decay $A \rightarrow VV$ (see (2)), we may evaluate ΔC_{VV} in the limit where the masses of these fermions are much larger than the masses of the external particles. Adding up the contributions of u_4, d_4, ℓ_4 , and ν_4 we obtain:

$$\Delta C_{WW} = \frac{i\alpha}{6\pi s_W^2} (\tan\beta + \cot\beta) \quad , \quad (18)$$

$$\Delta C_{ZZ} = \frac{i\alpha}{6\pi s_W^2} (1 - 3s_W^2 + 4s_W^4) (\tan\beta + \cot\beta) \quad . \quad (19)$$

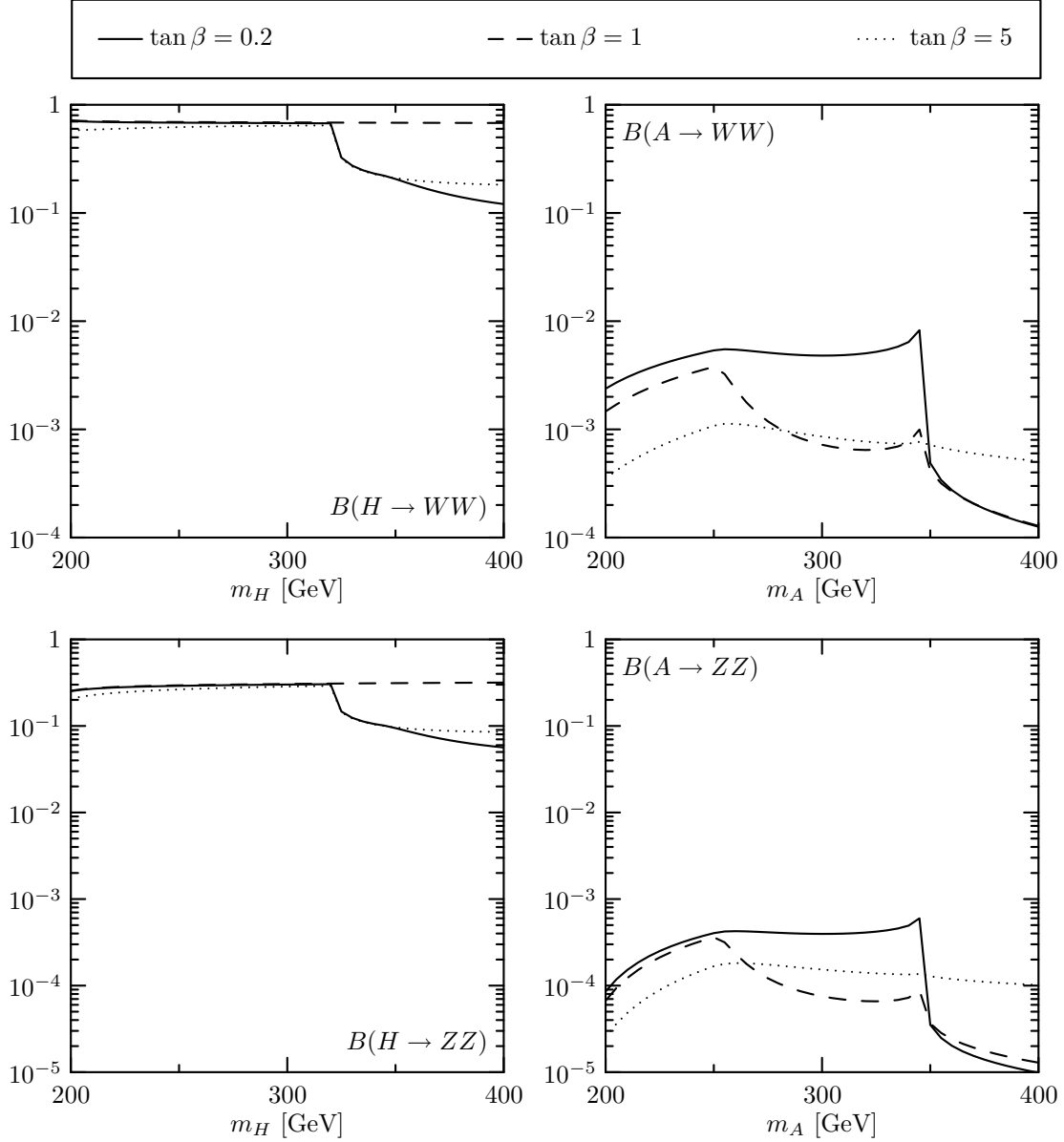


Figure 9: Heavy Higgs-boson branching ratios in the 2HDM with a fourth generation of chiral fermions. Shown are the branching ratios of H (left column) and A (right column) into WW (first row) and ZZ (second row) as functions of the decaying particle's mass for different values of $\tan\beta$. The remaining parameters are as given in the text.

For the masses chosen above and in Fig. 9, these formulae are in fact reasonable approximations to the exact one-loop amplitudes. That is, the values for $B(A, H \rightarrow VV)$ shown in Fig. 9 apply also to much heavier fourth-generation fermions.

Eq. 18 and 19 imply that u_4, d_4, ℓ_4, ν_4 make a significant contribution to the partial widths $\Gamma(A \rightarrow VV)$, especially for small or large $\tan\beta$. These widths are larger than those in the three-generation 2HDM of Sect. 2.1. On the other hand, u_4 and d_4 increase also the partial width $\Gamma(A \rightarrow gg)$ as compared to the three-generation 2HDM, which dominates the total width Γ_A for small $\tan\beta$. For large $\tan\beta$ and the above choice of masses, $A \rightarrow b\bar{b}$ makes the most significant contribution to Γ_A , as is the case in the three-generation 2HDM. Thus the branching ratios $B(A \rightarrow VV)$ shown in Fig. 9 are, for small $\tan\beta$, of similar size as those in the three-generation 2HDM shown in Fig. 4, but are much larger than the corresponding ones in Fig. 4 for large $\tan\beta$.

The branching ratios of $H \rightarrow VV$ lie between 20% and 70% for $m_H \leq 2m_h$. For extreme values of $\tan\beta$ they decrease rapidly when the $H \rightarrow hh$ decay channel opens. As in the three-generation 2HDM this feature relies on the fact that the Hhh vertex is enhanced by $1/\sin 2\beta$. For large $\tan\beta$ the $H \rightarrow VV$ branching ratios drop again by a factor of 2 when the $H \rightarrow t\bar{t}$ channel opens, since this channel is enhanced for large $\tan\beta$. The behaviour of the total widths at these thresholds is essentially the same as in the 3-generation 2HDM shown in Fig. 5.

In summary, the A branching ratios do not exceed 10^{-2} for the WW and 10^{-3} for the ZZ final state. The ratios R_W and R_Z can reach 10% and 1%, respectively, if the $H \rightarrow hh$ channel is open and enhanced but the decay $A \rightarrow t\bar{t}$ is kinematically forbidden.

2.4 Vector-like Quarks

A more exotic possibility for new heavy fermions are vector-like quarks, i.e., quarks whose left- and right-chiral components have equal gauge charges (see, e.g. [33, 34, 35, 36]). Such states are present in a number of SM extensions, including extra dimensional models with bulk fermions [37] and Little Higgs models [38]. Quarks of this type may exist with masses as low as a few hundred GeV; electroweak precision observables imply only very mild constraints [39].

Here we extend the three-generation 2HDM by multiplets of vector-like quarks along the lines of [34]. We add a $SU(2)_L$ doublet $Q = (U, D)$ with hypercharge 1/6 and two singlets D' and U' with hypercharges 2/3 and $-1/3$, respectively. The couplings of the vector-quarks to the electroweak gauge bosons are given by the $SU(2)_L \times U(1)_Y$ -invariant Lagrangian

$$\mathcal{L}_{\text{VQ,gauge}} = \bar{Q}i\cancel{D}Q + \bar{U}'i\cancel{D}U' + \bar{D}'i\cancel{D}D' - M_Q\bar{Q}Q - M_{U'}\bar{U}'U' - M_{D'}\bar{D}'D' \quad , \quad (20)$$

where \cancel{D} denotes the covariant derivative. The explicit mass terms are allowed because the left- and right-handed components of the vector-quarks transform under the same

representation of the electroweak gauge group. We construct the Yukawa interactions of the vector-like quarks with two Higgs doublets $\Phi_u = (\phi_u^+, \phi_u^0)$ and $\Phi_d = (\phi_d^+, \phi_d^0)$ in analogy to the chiral quark sector of the type-II 2HDM, i.e.,

$$\mathcal{L}_{\text{VQ,Yuk}} = -y_{U'}\bar{Q}_L\Phi_u^c U'_R - y_{D'}\bar{Q}_L\Phi_d D'_R - \tilde{y}_{U'}\bar{Q}_R\Phi_u^c U'_L - \tilde{y}_{D'}\bar{Q}_R\Phi_d D'_L + \text{h.c.} \quad , \quad (21)$$

with $\Phi_{u,d}^c = i\sigma_2\Phi_{u,d}^*$. The Yukawa couplings $y_{U'}$, $y_{D'}$, $\tilde{y}_{U'}$ and $\tilde{y}_{D'}$ can, in general, be complex⁶. As we are not interested here in CP-violating effects, we take all Yukawa couplings to be real. Then observables are invariant under the following parameter transformations:

$$\begin{aligned} (y_{U'}, \tilde{y}_{U'}, y_{D'}, \tilde{y}_{D'}) &\rightarrow (-y_{U'}, -\tilde{y}_{U'}, y_{D'}, \tilde{y}_{D'}) \quad , \\ (y_{U'}, \tilde{y}_{U'}, y_{D'}, \tilde{y}_{D'}) &\rightarrow (y_{U'}, \tilde{y}_{U'}, -y_{D'}, -\tilde{y}_{D'}) \quad , \\ (y_{U'}, \tilde{y}_{U'}, y_{D'}, \tilde{y}_{D'}) &\rightarrow (\tilde{y}_{U'}, y_{U'}, \tilde{y}_{D'}, y_{D'}) \quad . \end{aligned} \quad (22)$$

Invariance of our model under the first two transformations can be shown by absorbing the signs into the definitions of the singlet fields U' and D' , respectively, while invariance under the last transformation follows from redefining the vector-quark fields by their parity-transformed counterparts ($U \rightarrow \gamma^0 U$, etc.).

When the Higgs doublets acquire vacuum expectation values $\langle\Phi_u\rangle = (0, v_u)$ and $\langle\Phi_d\rangle = (0, v_d)$ we obtain the following mass terms for the vector-quarks:

$$\begin{aligned} \mathcal{L}_{\text{VQ,mass}} &= -y_{U'}v_u\bar{U}_L U'_R - y_{D'}v_d\bar{D}_L D'_R - \tilde{y}_{U'}v_u\bar{U}'_L U_R - \tilde{y}_{D'}v_d\bar{D}'_L D_R \\ &\quad - M_Q\bar{U}_L U_R - M_Q\bar{D}_L D_R - M_{U'}\bar{U}'_L U'_R - M_{D'}\bar{D}'_L D'_R + \text{h.c.} \\ &= -\begin{pmatrix} \bar{U}_L \\ \bar{U}'_L \end{pmatrix}^\top \begin{pmatrix} M_Q & y_{U'}v_u \\ \tilde{y}_{U'}v_u & M_{U'} \end{pmatrix} \begin{pmatrix} U_R \\ U'_R \end{pmatrix} \\ &\quad - \begin{pmatrix} \bar{D}_L \\ \bar{D}'_L \end{pmatrix}^\top \begin{pmatrix} M_Q & y_{D'}v_d \\ \tilde{y}_{D'}v_d & M_{D'} \end{pmatrix} \begin{pmatrix} D_R \\ D'_R \end{pmatrix} + \text{h.c.} \quad . \end{aligned} \quad (23)$$

The mass matrices can be diagonalised by independent rotations of the left- and right-handed components of the vector-quarks. Substituting

$$\begin{aligned} \begin{pmatrix} D \\ D' \end{pmatrix}_{L,R} &= \begin{pmatrix} \cos\varphi_{L,R}^D & -\sin\varphi_{L,R}^D \\ \sin\varphi_{L,R}^D & \cos\varphi_{L,R}^D \end{pmatrix} \begin{pmatrix} D_1 \\ D_2 \end{pmatrix}_{L,R} \quad , \\ \begin{pmatrix} U \\ U' \end{pmatrix}_{L,R} &= \begin{pmatrix} \cos\varphi_{L,R}^U & -\sin\varphi_{L,R}^U \\ \sin\varphi_{L,R}^U & \cos\varphi_{L,R}^U \end{pmatrix} \begin{pmatrix} U_1 \\ U_2 \end{pmatrix}_{L,R} \quad , \end{aligned} \quad (24)$$

⁶Three of the complex phases can be absorbed by redefining the vector-quark fields Q , U' and D' . The remaining phase may be absorbed into one of the Higgs doublets, but then it introduces, in general, CP violation in the Higgs sector.

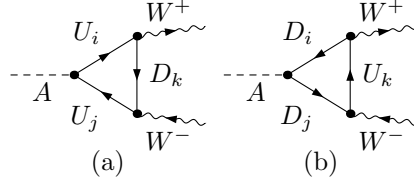


Figure 10: Vector-quark contributions to the $A \rightarrow WW$ decay amplitude. The indices i , j and k run from 1 to 2.

one sees that the mass matrices become diagonal if

$$\begin{aligned}
 t_{L-R}^{U,D} &\equiv \tan(\varphi_L^{U,D} - \varphi_R^{U,D}) = \frac{v_{u,d}(\tilde{y}_{U',D'} - y_{U',D'})}{M_Q + M_{U',D'}} \quad , \\
 t_{L+R}^{U,D} &\equiv \tan(\varphi_L^{U,D} + \varphi_R^{U,D}) = \frac{v_{u,d}(\tilde{y}_{U',D'} + y_{U',D'})}{M_Q - M_{U',D'}} \quad .
 \end{aligned} \tag{25}$$

The mass eigenvalues are

$$\begin{aligned}
 m_{U_{1,2}} &= \frac{1}{2} \left[\sqrt{(M_Q + M_{U'})^2 + v_u^2(y_{U'} - \tilde{y}_{U'})^2} \pm \sqrt{(M_Q - M_{U'})^2 + v_u^2(y_{U'} + \tilde{y}_{U'})^2} \right] \quad , \\
 m_{D_{1,2}} &= \frac{1}{2} \left[\sqrt{(M_Q + M_{D'})^2 + v_d^2(y_{D'} - \tilde{y}_{D'})^2} \pm \sqrt{(M_Q - M_{D'})^2 + v_d^2(y_{D'} + \tilde{y}_{D'})^2} \right] \quad .
 \end{aligned} \tag{26}$$

The couplings of the pseudoscalar Higgs boson A and of the W and Z bosons to the mass eigenstate vector-quarks $U_{1,2}$, $D_{1,2}$ are given in appendix A.

For the $A \rightarrow WW, ZZ$ partial widths there are several suppression mechanisms at work here. First note that for $y_{U',D'} = \pm \tilde{y}_{U',D'}$ the Yukawa interactions of the vector-quarks become parity-conserving⁷ and, therefore, they do not contribute to $A \rightarrow WW, ZZ$ at one-loop. If both $\tilde{y}_{U',D'} - y_{U',D'}$ and $\tilde{y}_{U',D'} + y_{U',D'}$ are large, (25) tells us that either $\varphi_L^{U,D}$ or $\varphi_R^{U,D}$ approaches 0 or $\pi/2$. Then many (but not necessarily all) diagrams of Fig. 10 and 11 get suppressed by sine or cosine factors of the mixing angles in the couplings.

The vector-quark contributions to $A \rightarrow WW$ and $A \rightarrow ZZ$ are shown in Fig. 10 and 11, respectively. In addition to the suppression mechanisms discussed above there are other cancellations. While the “diagonal” couplings between A and the vector-quarks ($AU_1\bar{U}_1$, $AD_1\bar{D}_1$ etc.) are pure pseudoscalar, the “off-diagonal” couplings ($AU_1\bar{U}_2$, $AD_1\bar{D}_2$ etc.) have scalar and pseudoscalar Lorentz structure. Yet the contributions of the scalar terms to the form factor $f_{3,VV'}$ from (1) must cancel, and this is seen by observing that these terms change sign if the fermion flow in the loop is reversed.

⁷If $y_{U',D'} = +\tilde{y}_{U',D'}$ this is immediately obvious. If $y_{U',D'} = -\tilde{y}_{U',D'}$ the minus signs can be absorbed into U'_R and D'_R .

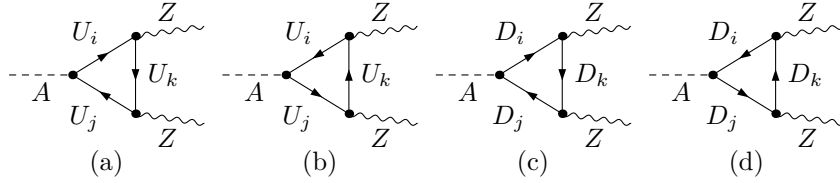


Figure 11: Vector-quark contributions to the $A \rightarrow ZZ$ decay amplitude. The indices i, j and k run from 1 to 2.

There are further cancellations between the pseudoscalar terms. For example, for $M_Q = M_{U'} = M_{D'}$ the $A \rightarrow ZZ$ diagrams with only one type of vector-quark in the loop cancel exactly in the limit of large M_Q .

To control the various suppression mechanisms, we invert (25) and (26) and use the following quantities as independent parameters:

$$M_Q, t_{L-R}^U, t_{L+R}^U, m_{U_2}, t_{L-R}^D, t_{L+R}^D, m_{D_2} \quad . \quad (27)$$

Using the invariance under the transformations (22) we may limit ourselves to the case

$$t_{L-R}^U, t_{L-R}^D, t_{L+R}^D > 0 \quad . \quad (28)$$

Note that t_{L+R}^U can still be negative.

Let us now come to the numerical analysis. Throughout the following discussion we set

$$\beta - \alpha = \frac{\pi}{4} \quad , \quad M_Q = 1 \text{ TeV} \quad . \quad (29)$$

Our choice for α assures that the HVV Born vertices are not suppressed. We will first discuss a scenario where the pseudoscalar Higgs boson is too light to decay into vector-quarks. In this case the leading contributions to the H and A total widths are again the decays (8). As in the case of the 2HDM with a 4th generation the contributions of the new heavy quarks to the partial widths of $H \rightarrow gg$ and $A \rightarrow gg$ have to be taken into account, too. We further distinguish between scenarios with small or large values of $\tan \beta$. The contributions of vector-quark loops to $A \rightarrow WW$ and $A \rightarrow ZZ$ decays generally saturate if the magnitude of the t parameters (25) is larger than 10. The biggest corrections were found for $t_{L-R}^D, t_{L+R}^D, t_{L-R}^U \gtrsim 10$ and $t_{L+R}^U \lesssim -10$. Unless stated otherwise, we therefore choose for our numerical analysis

$$m_{U_2} = m_{D_2} = 320 \text{ GeV}, \quad t_{L-R}^D = t_{L+R}^D = t_{L-R}^U = 10, \quad t_{L+R}^U = -10. \quad (30)$$

Fig. 12 shows, for $m_A = 250 \text{ GeV}$, the $A \rightarrow WW$ and $A \rightarrow ZZ$ branching ratios as functions of t_{L-R}^U for $\tan \beta = 0.2$ and different values of t_{L+R}^U . Note that for small values of $\tan \beta$ the couplings between A and the D -type vector-quarks are suppressed. As a result, only the diagrams with U -type vector-quarks are relevant for the $A \rightarrow ZZ$ decay

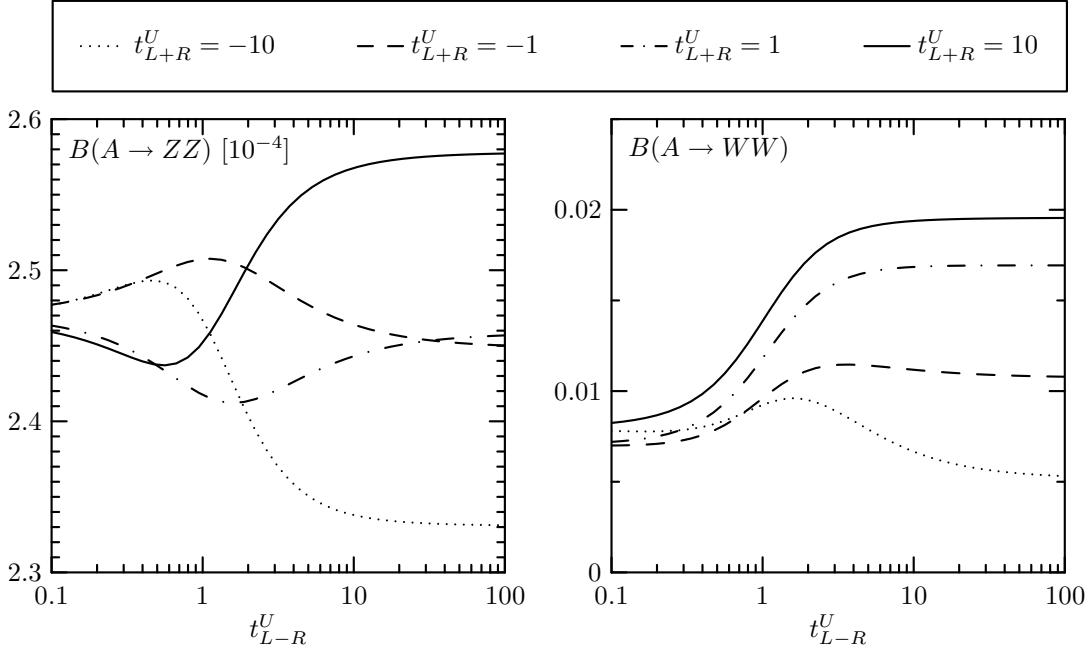


Figure 12: Results for the $A \rightarrow ZZ$ (left) and $A \rightarrow WW$ (right) branching ratios in the 2HDM with vector-quarks for the parameters from (29) and (30), $m_A = 250$ GeV, $\tan \beta = 0.2$ and different values of t_{L+R}^U as functions of t_{L-R}^U .

in this case and the partial width only depends on the U -type t parameters t_{L+R}^U and t_{L-R}^U . The biggest contribution to the $A \rightarrow ZZ$ partial width is, however, due to the top-quark loop, while the contributions from vector-quark loops are one order of magnitude smaller. Consequently the value of the branching ratio is almost the same as the one in Sect. 2.1 and the dependence on the t parameters is very weak. The smallness of the vector-quark corrections to the $A \rightarrow ZZ$ decay is mainly due to the relation between the Yukawa couplings and the mixing angles: whenever a Yukawa coupling gets large, some other mixing-angle dependent factor in the couplings gets small.

For the WW final state the diagrams contain both U and D -type vector-quarks and therefore depend on the U -type mixing angles, too. For large Yukawa couplings the vector-quark contributions to the $A \rightarrow WW$ decay are then dominated by just a few diagrams, where the suppression by mixing angles can be avoided altogether. As a result they can be much larger than the corrections to the $A \rightarrow ZZ$ decay. For small $\tan \beta$ they can be of the same order as the contributions from SM fermion loops. As Fig. 12 shows, the branching ratio can then reach up to about 2%, i.e. more than twice its corresponding value in the 2HDM of Sect. 2.1. For both the ZZ and WW final state we observe that the vector-quark loop contributions can partially cancel the contributions from SM fermion loops for $t_{L+R}^U < 0$, while for $t_{L+R}^U > 0$ they always add.

As discussed in Sect. 2.1, the contributions of SM fermion loops to the $A \rightarrow WW, ZZ$ partial widths drop by several orders of magnitude if we increase $\tan \beta$. Like in the

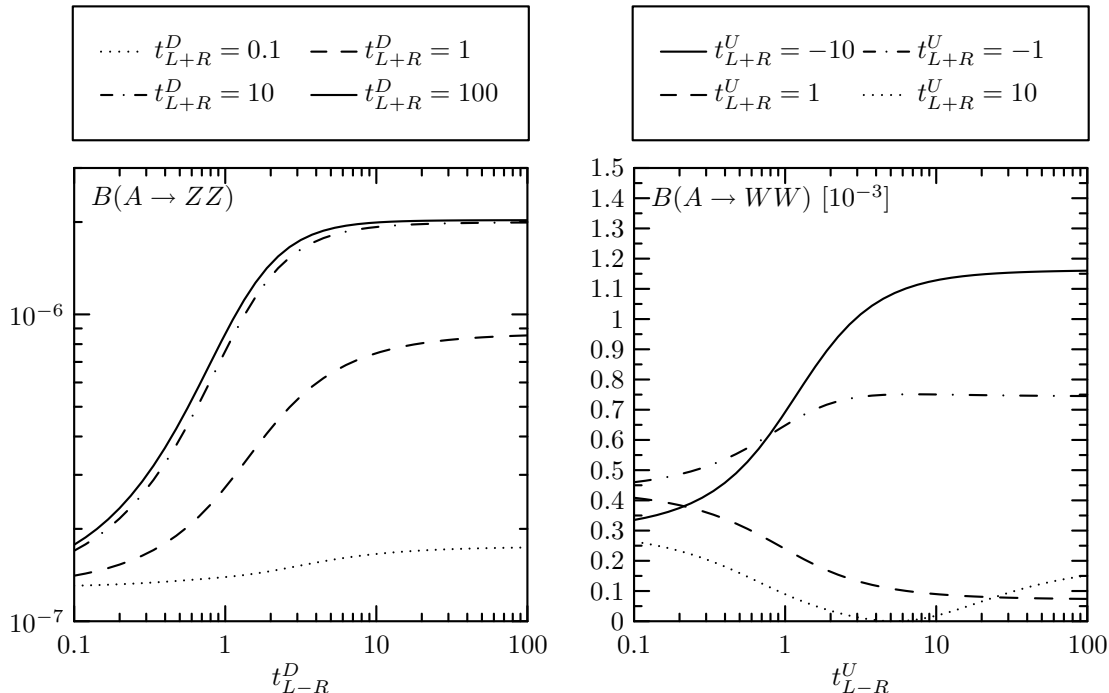


Figure 13: Results for $A \rightarrow WW, ZZ$ branching ratios in the 2HDM with vector-quarks for $m_A = 250$ GeV, $\tan \beta = 5$ and the parameters from (29) and (30). Left: the $A \rightarrow ZZ$ branching ratio for different values of t_{L+R}^D as functions of t_{L-R}^D . Right: the $A \rightarrow WW$ branching ratio for different values of t_{L+R}^U as functions of t_{L-R}^U .

2HDM with a 4th generation of chiral fermions, the contributions of the vector-quark loops get large for small and large values of $\tan \beta$ if the U and D -type vector-quark masses are of the same order. Consequently, for large $\tan \beta$, the dominant contributions to the $A \rightarrow WW, ZZ$ partial widths come from the vector-quark loops. Fig. 13 shows the $A \rightarrow WW, ZZ$ branching ratios for $\tan \beta = 5$. Here the contributions from diagrams where the A couples to U -type vector-quarks are negligible and consequently the $A \rightarrow ZZ$ branching ratio is insensitive to the U -type t parameters t_{L+R}^U and t_{L-R}^U . The left plot in Fig. 13 shows the branching ratio for $A \rightarrow ZZ$ as a function of t_{L-R}^D for different values of t_{L+R}^D . It does not exceed 2×10^{-6} .

The right plot in Fig. 13 shows the branching ratio for $A \rightarrow WW$ as a function of t_{L-R}^U for different values of t_{L+R}^U . The branching ratio gets largest for $t_{L+R}^U < -10$ and $t_{L+R}^U, t_{L-R}^U > 10$ and reaches approximately 0.12%. The dominant diagram for $t_{L+R}^U < 0$ is diagram (b) from Fig. 10 with $(i, j, k) = (1, 1, 2)$. For $t_{L+R}^U > 0$ it is diagram (b) with $i = j = k = 1, 2$. By varying t_{L+R}^D and t_{L-R}^D the scale of the curves changes while their shape stays essentially the same. However, the resulting values of the branching ratios do not exceed $\sim 0.12\%$. As for the dependence on particle masses we observe that the $A \rightarrow WW$ partial width is virtually independent of the lightest vector-quark masses m_{U_2} and m_{D_2} , while the partial width for the ZZ final state increases by one order of magnitude if we set $m_{D_2} = 200$ GeV. Again, the shapes of the curves in the left plot of

Fig. 13 stay the same if we change m_{D_2} .

Let us now have a look at the dependence of the branching ratios on the mass of the decaying particles. We will only discuss the case $\tan\beta = 5$ where the $A \rightarrow WW, ZZ$ partial widths are dominated by vector-quark loops. For small $\tan\beta$ these contributions show a similar behaviour, and the m_A dependence of the SM fermion loop contributions was discussed in Sect. 2.1. The curves of Fig. 13 simply scale if we change m_A while their shape stays essentially the same. It is therefore sufficient to plot the A branching ratios as functions of m_A for a few selected combinations of the parameters (27). Fig. 14 shows the A and H branching ratios into WW and ZZ for the assignments (29), $m_{U_2} = m_{D_2} = 320$ GeV, and different combinations of the t parameters.

Sufficiently heavy H, A will also decay into the lightest U - and D -type vector-quarks: $H, A \rightarrow U_2\bar{U}_2, D_2\bar{D}_2$. For large $\tan\beta$ the decay $H \rightarrow U_2\bar{U}_2$ decay is strongly suppressed and the total width of H depends only on the D -type t parameters. As a result the three graphs for $B(H \rightarrow WW)$ are essentially identical because t_{L+R}^D and t_{L-R}^D are held fixed in the right column of Fig. 14. Below the vector-quark threshold the $H \rightarrow ZZ$ branching ratio depends on the t parameters only through the contributions of vector-quark mediated $H \rightarrow gg$ decays to the total width. Since the $H \rightarrow gg$ channel is subdominant for large $\tan\beta$, the $H \rightarrow ZZ$ branching ratio is not very sensitive to the t parameters below the vector-quark threshold. Above that threshold it drops off more quickly for small values of t_{L+R}^D . Furthermore, the $H \rightarrow WW$ and $H \rightarrow ZZ$ branching ratios both drop by one order of magnitude at $m_H = 320$ GeV. This corresponds to the opening of the $H \rightarrow hh$ decay channel, which is strongly enhanced by the factor $1/\sin(2\beta)$ in the Hhh vertex. As already discussed in Sect. 2.1, this enhancement is not a necessary feature of the model. The ratios $B(A \rightarrow WW, ZZ)$ drop by an order of magnitude for $m_A > 2m_{Q_2}$.

Fig. 15 shows the total widths of H and A as a function of $m_{H,A}$ for $\tan\beta = 5$. As we have allowed for an enhanced Hhh coupling, the width Γ_H increases rapidly for $m_H > 2m_h$. The width Γ_A of the pseudoscalar $\Gamma_A \lesssim 20$ GeV below the vector-quark production threshold which we put $2m_{Q_2} = 640$ GeV. Above this threshold and for strong $AQ_2\bar{Q}_2$ coupling, Γ_A increases dramatically and the perturbative result displayed in Fig. 15 becomes unreliable. Yet, we emphasize that a significantly higher $Q_2\bar{Q}_2$ threshold would not change our results on $B(H, A \rightarrow VV)$ below $m_{H,A} \leq 2m_{Q_2}$ in an essential way.

In summary, for $\tan\beta = 5$ we find $B(A \rightarrow WW) \lesssim 10^{-3}$ and $B(A \rightarrow ZZ) \lesssim 10^{-4}$. As shown above $B(A \rightarrow WW)$ can become an order of magnitude larger for $\tan\beta \sim 0.2$. The ratio R_W can become $\sim 10\%$ if the $H \rightarrow hh$ channel is open and enhanced but the decay $A \rightarrow t\bar{t}$ is kinematically forbidden.

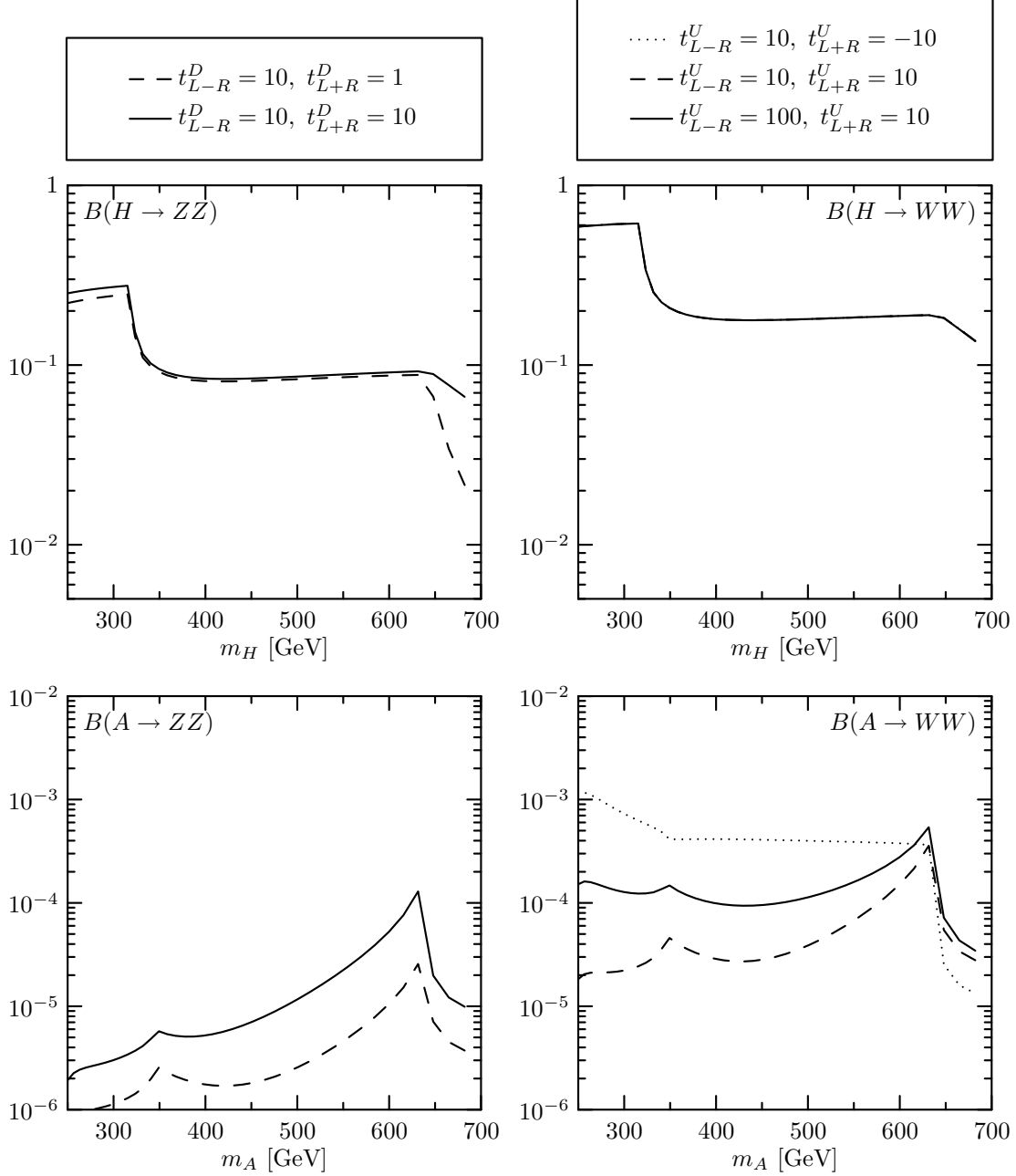


Figure 14: The H (first row) and A (second row) branching ratios in the 2HDM with vector-quarks for $\tan\beta = 5$ and the parameters from (29) and (30) as functions of the mass of the decaying particle. Left column: the branching ratios for the ZZ final state for different combinations of t_{L+R}^D and t_{L-R}^D . Right column: the branching ratio for the WW final state for different combinations of t_{L+R}^U and t_{L-R}^U . In the plot for $B(H \rightarrow WW)$ all three graphs lie on top of each other.

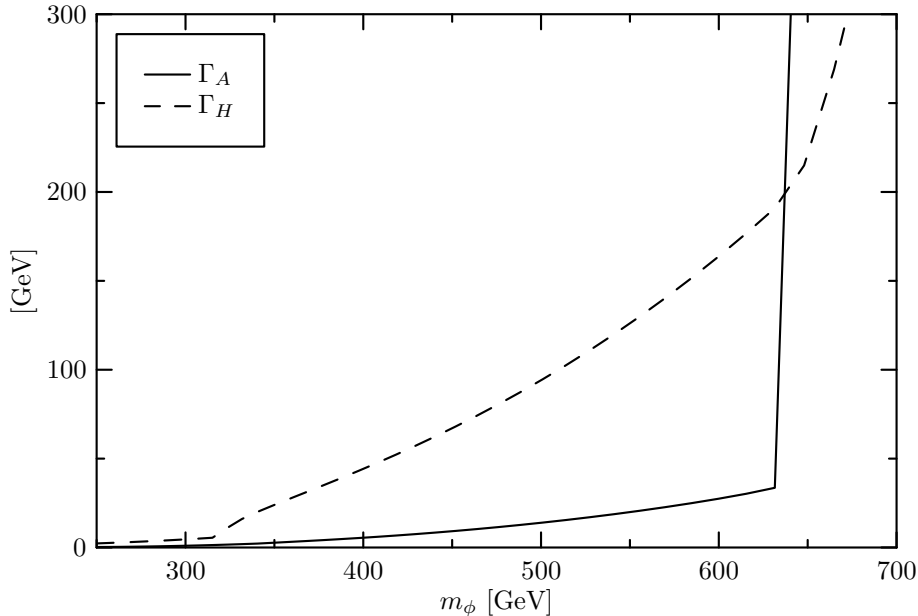


Figure 15: The total widths of H and A in the 2HDM with vector-quarks for $\tan\beta = 5$ and the parameters from (29) and (30) as functions of the particle mass.

2.5 Top-color assisted technicolor

An alternative to the Higgs mechanism is EWSB triggered by the condensation of (new) fermion antifermion pairs. Phenomenologically viable models of this type include models based on the concept of top-color assisted technicolor (TC2) [4, 18]. These models have two strongly interacting sectors in order to explain EWSB and the large top-quark mass. Technicolor interactions (TC) are responsible, via the condensation of techni-fermions, $\langle \bar{T}T \rangle$ ($T = U, D$), for most of EWSB, but they contribute very little to the top-quark mass m_t , while top-color interactions generate through condensation of top-quark pairs, $\langle \bar{t}t \rangle$, the bulk of m_t but make only a small contribution to EWSB. The spin-zero states of the model are bound-states of the techni-fermions and of t, b . These two sets of bound-states form two $SU(2)_L$ doublets Φ_{TC}, Φ_t , whose couplings to the weak gauge bosons and to t and b are formally equivalent to those of a two-Higgs doublet model. The physical spin-zero states are i) a heavy neutral scalar H_{TC} with a mass of order 1 TeV, ii) a neutral scalar H_t which is a $\bar{t}t$ bound state whose mass is expected to be of the order $m_{H_t} \sim 2m_t$ when estimated à la Nambu-Jona-Lasinio, but could in fact be lighter [40], and iii) a neutral “top-pion” Π^0 and a pair of charged ones, Π^\pm , whose masses are predicted to lie in the range of 200 - 300 GeV [18, 41].

The couplings of spin-zero states to the weak gauge bosons and to the t and b quarks can be obtained from an effective $SU(2)_L \times U(1)_Y$ invariant Lagrangian involving the

m_ϕ [GeV]:	200	300
Γ_{H_t} [GeV]:	0.072	0.375
Γ_{Π^0} [GeV]:	0.088	0.500

Table 1: The total widths of $\phi = H_t, \Pi^0$ for two values of m_ϕ and $f_\pi = 40$ GeV.

doublets Φ_{TC}, Φ_t [42]. The interactions of the top quark with H_t and Π^0 are given by:

$$\mathcal{L}_{Y,t} = -\frac{Y_t}{\sqrt{2}}\bar{t}t H_t - \frac{Y_\pi}{\sqrt{2}}\bar{t}i\gamma_5 t \Pi^0 \quad , \quad (31)$$

where $Y_\pi = (Y_t v_T - \varepsilon_t f_\pi)/v$ and $(Y_t f_\pi + \varepsilon_t v_T)/\sqrt{2} = m_t$. Here f_π denotes the value of the top-quark condensate which is estimated in the TC2 model to lie between 40 GeV $\lesssim f_\pi \lesssim 80$ GeV [18, 42]. Once f_π is fixed, v_T is determined by the EWSB requirement that $f_\pi^2 + v_T^2 = v^2 = (246 \text{ GeV})^2$. The parameter ε_t denotes the technicolor contribution to the top mass which is small, by construction of the TC2 model, and we may henceforth safely put $\varepsilon_t = 0$. The large top-quark mass thus amounts to large top Yukawa couplings Y_t, Y_π , e.g., $Y_t \simeq Y_\pi \simeq 4$ for $f_\pi \simeq 60$ GeV. The couplings of H_t and Π^0 to b quarks are, on the other hand, significantly suppressed as compared with the SM Higgs $b\bar{b}$ coupling. By construction, the top-color interactions do not generate a direct contribution to the mass of the b quark. The bulk of m_b is assumed to be due to technicolor interactions. Disregarding top-color instanton effects, the tree-level $H_t b\bar{b}$ coupling is in fact zero, and the coupling of Π^0 to b quarks is given by

$$\mathcal{L}_{Y,b} = -\varepsilon_b \frac{f_\pi}{\sqrt{2}v} \bar{b}i\gamma_5 b \Pi^0 \quad , \quad (32)$$

where $\varepsilon_b = m_b \sqrt{2}/v_T$. With $m_b = 4.8$ GeV and $f_\pi \leq 80$ GeV one gets $\varepsilon_b \leq 0.03$.

In the following we consider top-pions $\Pi^{0,\pm}$ with masses $m_{\Pi^0} = m_{\Pi^\pm}$ in the range between 200 GeV and 400 GeV and choose, for reasons of comparison, the mass of H_t to lie in the same range. As the ‘‘technicolor Higgs’’ boson H_{TC} is much heavier than $\Pi^{0,\pm}$ and H_t , it plays no role in the decays of Π^0 and H_t .

While the decays $H_t \rightarrow WW, ZZ$ occur already at Born level with couplings $h_{WW} = h_{ZZ} = f_\pi/v$ (cf. Eq. 4), the corresponding decays of Π^0 are loop-induced and the amplitudes are completely dominated by the strong $\Pi^0 \bar{t}t$ coupling, i.e., by the diagrams that correspond to Fig. 1 (b) and 2 (b), respectively. This is also the case for the $H_t, \Pi^0 \rightarrow gg$ decays. As emphasized above the decays $\Pi^0 \rightarrow b\bar{b}$ are strongly suppressed and $H_t \rightarrow b\bar{b}$ is absent at tree-level.

For $m_\Pi \leq 2m_t$ the total rate Γ_{Π^0} , given in Table 1, is dominated by $\Pi^0 \rightarrow gg$. Below the $t\bar{t}$ threshold the channel $H_t \rightarrow gg$ contributes also a significant portion to Γ_{H_t} . If $2m_V < m_{H_t} \leq 2m_t$ then $B(H_t \rightarrow gg) \leq 45\%$ for $f_\pi \geq 40$ GeV.

As a consequence of these features, the branching ratios $B(\Pi^0 \rightarrow WW, ZZ)$ are essentially independent of f_π , while $B(H_t \rightarrow WW, ZZ)$ increase with increasing f_π , namely by about a factor of two if f_π is changed from 40 GeV to 80 GeV.

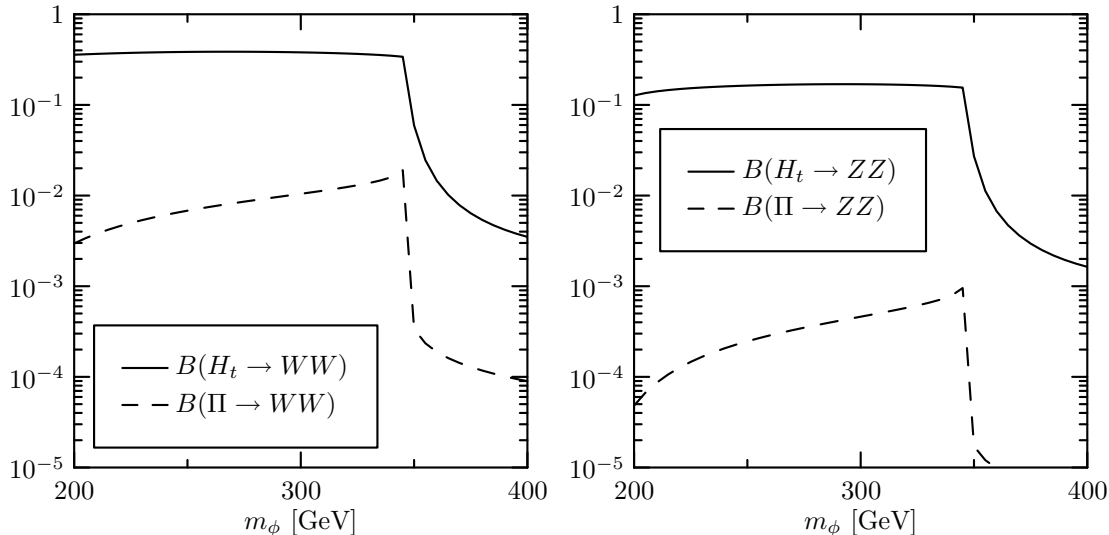


Figure 16: The TC2 branching ratios of the decays of Π^0 and H_t into WW (left) and ZZ (right) final states as functions of the respective mass ($\phi = \Pi^0, H_t$), for $f_\pi = 40$ GeV.

Fig. 16 shows the branching ratios $B(H_t, \Pi^0 \rightarrow WW/ZZ)$ as functions of the mass of the respective spin zero resonance, for $f_\pi = 40$ GeV. Once the $t\bar{t}$ threshold is crossed, there are sharp drops, because the decays into $t\bar{t}$ then dominate the total widths of both Π^0 and H_t . For masses below the $t\bar{t}$ threshold, which are preferred by model predictions [18, 41], we thus obtain $B(\Pi^0 \rightarrow WW) \lesssim 2 \times 10^{-2}$, $B(\Pi^0 \rightarrow ZZ) \lesssim 10^{-3}$ and the ratios $R_W \lesssim 0.07$, $R_Z \lesssim 0.007$.

3 Summary and Conclusions

In this paper we addressed two questions: Assuming the existence of a non-standard EWSB sector with a spin-0 (Higgs) resonance spectrum which includes a pseudoscalar A with mass $m_A \gtrsim 200$ GeV, we investigated whether the decays $A \rightarrow WW/ZZ$ can have branching ratios at the percent level and analysed the size of $B(A \rightarrow WW/ZZ)$ relative to the respective branching ratio of a scalar boson H with mass $m_H \simeq m_A$. We analyzed this in the context of the MSSM, in non-supersymmetric type-II two-Higgs doublet extensions of the SM without and with additional heavy fermions, and in TC2.

For the MSSM we confirmed what is known in the literature, i.e., that the $A \rightarrow WW/ZZ$ are rare. But also the branching ratios $B(H \rightarrow WW/ZZ)$ can be below the per mill level in the scenario discussed in Sect. 2.2. In the three-generation 2HDM and in the corresponding models with an additional 4th sequential fermion generation or heavy vector-like quarks the branching ratio $B(A \rightarrow WW)$ can reach about 2% for $m_A \leq 2m_t$, while $B(A \rightarrow ZZ) \lesssim 10^{-3}$. In this case the total width Γ_A is dominated by $A \rightarrow gg$ and $A \rightarrow Zh$ (if kinematically possible) while $A \rightarrow b\bar{b}, \tau^-\tau^+$ are suppressed. The tree-level

couplings HVV can be severely suppressed, which implies small $B(H \rightarrow WW/ZZ)$ and ratios $R_{W,Z}$ (5) of order one – but this amounts to fine-tuned parameters α and β . Even if the HVV Born couplings are not suppressed, $B(H \rightarrow WW)$ and $B(H \rightarrow ZZ)$ may not exceed $\sim 10\%$ below the $t\bar{t}$ threshold if $H \rightarrow hh$ is kinematically possible and enhanced. In TC2 models the latter decay mode is absent. If a composite scalar resonance H_t below the $t\bar{t}$ threshold exists, it will predominantly decay into gg, WW, ZZ . We obtain $B(H_t \rightarrow WW) \lesssim 0.4$ and $B(H_t \rightarrow ZZ) \lesssim 0.1$. The neutral pseudoscalar resonance Π^0 with $m_\Pi \leq 2m_t$ decays dominantly into gluons; $B(\Pi^0 \rightarrow WW) \lesssim 0.02$ and $B(\Pi^0 \rightarrow ZZ) \lesssim 10^{-3}$.

In view of these results one may resume the issue raised in the introduction, whether the discovery of a spin-zero resonance ϕ in the WW and/or ZZ channel allows the conclusion that this particle has $J^{PC} = 0^{++}$ – prior to performing the tests proposed in [3, 10, 11, 12, 13, 14, 15, 16, 17]. Our findings suggest the following: If $\phi \rightarrow WW, ZZ$ are dominant decay channels then it is very likely that ϕ is a scalar. If these modes are suppressed as compared to other channels, there is a non-negligible probability that ϕ is a pseudoscalar. Of course, these CP tests – and other CP tests in $\phi \rightarrow t\bar{t}, \tau^-\tau^+$ (see .e.g., [3, 43, 44]) – are eventually indispensable in order to establish whether or not ϕ is a true CP eigenstate.

Acknowledgments

This work was supported by Deutsche Forschungsgemeinschaft SFB/TR9.

A Feynman Rules for the Vector-Quark Model

In this appendix we list the Feynman rules for the 2HDM model with vector-like quarks, which we discussed in section 2.4. We list only the couplings of vector-quarks to H, A, W and Z . In the rules given, all particles flow into the vertex. In the case where two vertices are related by a hermitian conjugation, only one representative is shown. As usual, $P_{R,L} = (1 \pm \gamma_5)/2$.

A.1 Yukawa Couplings of H to Vector-Quarks

$H U_2 \bar{U}_2$:

$$\frac{is_\alpha}{\sqrt{2}}(c_R^U s_L^U y_U + c_L^U s_R^U \tilde{y}_U)$$

$H U_2 \bar{U}_1$:

$$\frac{is_\alpha}{\sqrt{2}}[(s_L^U s_R^U y_U - c_L^U c_R^U \tilde{y}_U)P_L + (-c_L^U c_R^U y_U + s_L^U s_R^U \tilde{y}_U)P_R]$$

$$H U_1 \bar{U}_1: \\ -\frac{is_\alpha}{\sqrt{2}}(c_L^U s_R^U y_U + c_R^U s_L^U \tilde{y}_U)$$

$$H D_2 \bar{D}_2: \\ \frac{ic_\alpha}{\sqrt{2}}(c_R^D s_L^D y_D + c_L^D s_R^D \tilde{y}_D)$$

$$H D_2 \bar{D}_1: \\ \frac{ic_\alpha}{\sqrt{2}}[(s_L^D s_R^D y_D - c_L^D c_R^D \tilde{y}_D)P_L + (-c_L^D c_R^D y_D + s_L^D s_R^D \tilde{y}_D)P_R]$$

$$H D_1 \bar{D}_1: \\ -\frac{ic_\alpha}{\sqrt{2}}(c_L^D s_R^D y_D + c_R^D s_L^D \tilde{y}_D)$$

A.2 Yukawa Couplings of A to Vector-Quarks

$$A U_2 \bar{U}_2: \\ \frac{c_\beta}{\sqrt{2}}(c_R^U s_L^U y_U - c_L^U s_R^U \tilde{y}_U)\gamma_5$$

$$A U_1 \bar{U}_2: \\ \frac{c_\beta}{\sqrt{2}}[(c_L^U c_R^U y_U + s_L^U s_R^U \tilde{y}_U)P_L + (s_L^U s_R^U y_U + c_L^U c_R^U \tilde{y}_U)P_R]$$

$$A U_1 \bar{U}_1: \\ \frac{c_\beta}{\sqrt{2}}(-c_L^U s_R^U y_U + c_R^U s_L^U \tilde{y}_U)\gamma_5$$

$$A D_2 \bar{D}_2: \\ \frac{s_\beta}{\sqrt{2}}(c_R^D s_L^D y_D - c_L^D s_R^D \tilde{y}_D)\gamma_5$$

$$A D_1 \bar{D}_2: \\ \frac{s_\beta}{\sqrt{2}}[(c_L^D c_R^D y_D + s_L^D s_R^D \tilde{y}_D)P_L + (s_L^D s_R^D y_D + c_L^D c_R^D \tilde{y}_D)P_R]$$

$$A D_1 \bar{D}_1: \\ \frac{s_\beta}{\sqrt{2}}(-c_L^D s_R^D y_D + c_R^D s_L^D \tilde{y}_D)\gamma_5$$

A.3 Couplings of W to Vector-Quarks

$W_\mu^+ D_2 \bar{U}_2$:

$$-\frac{ie}{\sqrt{2}s_W}\gamma_\mu(s_L^D s_L^U P_L + s_R^D s_R^U P_R)$$

$W_\mu^+ D_1 \bar{U}_2$:

$$\frac{ie}{\sqrt{2}s_W}\gamma_\mu(c_L^D s_L^U P_L + c_R^D s_R^U P_R)$$

$W_\mu^+ D_2 \bar{U}_1$:

$$\frac{ie}{\sqrt{2}s_W}\gamma_\mu(c_L^U s_L^D P_L + c_R^U s_R^D P_R)$$

$W_\mu^+ D_1 \bar{U}_1$:

$$-\frac{ie}{\sqrt{2}s_W}\gamma_\mu(c_L^D c_L^U P_L + c_R^D c_R^U P_R)$$

A.4 Couplings of Z to Vector-Quarks

$Z_\mu U_2 \bar{U}_2$:

$$\frac{ie}{c_W s_W}\gamma_\mu\left[\left(\frac{2}{3}s_W^2 - \frac{1}{2}(s_L^U)^2\right)P_L + \left(\frac{2}{3}s_W^2 - \frac{1}{2}(s_R^U)^2\right)P_R\right]$$

$Z_\mu U_1 \bar{U}_2$:

$$\frac{ie}{2c_W s_W}\gamma_\mu(c_L^U s_L^U P_L + c_R^U s_R^U P_R)$$

$Z_\mu U_1 \bar{U}_1$:

$$\frac{ie}{c_W s_W}\gamma_\mu\left[\left(\frac{2}{3}s_W^2 - \frac{1}{2}(c_L^U)^2\right)P_L + \left(\frac{2}{3}s_W^2 - \frac{1}{2}(c_R^U)^2\right)P_R\right]$$

$Z_\mu D_2 \bar{D}_2$:

$$-\frac{ie}{c_W s_W}\gamma_\mu\left[\left(\frac{1}{3}s_W^2 - \frac{1}{2}(s_L^D)^2\right)P_L + \left(\frac{1}{3}s_W^2 - \frac{1}{2}(s_R^D)^2\right)P_R\right]$$

$$Z_\mu D_1 \bar{D}_2:$$

$$-\frac{ie}{2c_W s_W} \gamma_\mu (c_L^D s_L^D P_L + c_R^D s_R^D P_R)$$

$$Z_\mu D_1 \bar{D}_1:$$

$$-\frac{ie}{c_W s_W} \gamma_\mu \left[\left(\frac{1}{3} s_W^2 - \frac{1}{2} (c_L^D)^2 \right) P_L + \left(\frac{1}{3} s_W^2 - \frac{1}{2} (c_R^D)^2 \right) P_R \right]$$

References

- [1] A. Djouadi, *Phys. Rept.* **457** (2008) 1–216, [arXiv:hep-ph/0503172](#).
- [2] A. Djouadi, *Phys. Rept.* **459** (2008) 1–241, [arXiv:hep-ph/0503173](#).
- [3] E. Accomando *et al.*, [arXiv:hep-ph/0608079](#).
- [4] C. T. Hill and E. H. Simmons, *Phys. Rept.* **381** (2003) 235–402, [arXiv:hep-ph/0203079](#).
- [5] A. Bredenstein, A. Denner, S. Dittmaier, and M. M. Weber, *JHEP* **02** (2007) 080, [arXiv:hep-ph/0611234](#).
- [6] S. Asai *et al.*, *Eur. Phys. J.* **C32S2** (2004) 19–54, [arXiv:hep-ph/0402254](#).
- [7] S. Abdullin *et al.*, *Eur. Phys. J.* **C39S2** (2005) 41–61.
- [8] A. Mendez and A. Pomarol, *Phys. Lett.* **B272** (1991) 313–318.
- [9] J. F. Gunion, H. E. Haber, and C. Kao, *Phys. Rev.* **D46** (1992) 2907–2917.
- [10] C. A. Nelson, *Phys. Rev.* **D37** (1988) 1220.
- [11] A. Soni and R. M. Xu, *Phys. Rev.* **D48** (1993) 5259–5263, [arXiv:hep-ph/9301225](#).
- [12] A. Skjold and P. Osland, *Phys. Lett.* **B311** (1993) 261–265, [arXiv:hep-ph/9303294](#).
- [13] V. D. Barger, K.-m. Cheung, A. Djouadi, B. A. Kniehl, and P. M. Zerwas, *Phys. Rev.* **D49** (1994) 79–90, [arXiv:hep-ph/9306270](#).
- [14] T. Arens and L. M. Sehgal, *Z. Phys.* **C66** (1995) 89–94, [arXiv:hep-ph/9409396](#).
- [15] S. Y. Choi, D. J. Miller, M. M. Muhlleitner, and P. M. Zerwas, *Phys. Lett.* **B553** (2003) 61–71, [arXiv:hep-ph/0210077](#).

- [16] C. P. Buszello, I. Fleck, P. Marquard, and J. J. van der Bij, *Eur. Phys. J.* **C32** (2004) 209–219, [arXiv:hep-ph/0212396](#).
- [17] R. M. Godbole, D. J. Miller, and M. M. Muhlleitner, *JHEP* **12** (2007) 031, [arXiv:0708.0458 \[hep-ph\]](#).
- [18] C. T. Hill, *Phys. Lett.* **B345** (1995) 483–489, [arXiv:hep-ph/9411426](#).
- [19] T. Hahn, *Comput. Phys. Commun.* **140** (2001) 418–431, [arXiv:hep-ph/0012260](#).
- [20] T. Hahn and C. Schappacher, *Comput. Phys. Commun.* **143** (2002) 54–68, [arXiv:hep-ph/0105349](#).
- [21] T. Hahn and M. Perez-Victoria, *Comput. Phys. Commun.* **118** (1999) 153–165, [arXiv:hep-ph/9807565](#).
- [22] T. Hahn and M. Rauch, *Nucl. Phys. Proc. Suppl.* **157** (2006) 236–240, [arXiv:hep-ph/0601248](#).
- [23] J. F. Gunion, H. E. Haber, G. L. Kane, and S. Dawson, *The Higgs Hunter's Guide*. Perseus Publishing, Cambridge, Mass., 2000.
- [24] P. Gambino and M. Misiak, *Nucl. Phys.* **B611** (2001) 338–366, [arXiv:hep-ph/0104034](#).
- [25] M. Frank *et al.*, *JHEP* **02** (2007) 047, [arXiv:hep-ph/0611326](#).
- [26] G. Degrossi, S. Heinemeyer, W. Hollik, P. Slavich, and G. Weiglein, *Eur. Phys. J.* **C28** (2003) 133–143, [arXiv:hep-ph/0212020](#).
- [27] S. Heinemeyer, W. Hollik, and G. Weiglein, *Eur. Phys. J.* **C9** (1999) 343–366, [arXiv:hep-ph/9812472](#).
- [28] S. Heinemeyer, W. Hollik, and G. Weiglein, *Comput. Phys. Commun.* **124** (2000) 76–89, [arXiv:hep-ph/9812320](#).
- [29] G. D. Kribs, T. Plehn, M. Spannowsky, and T. M. P. Tait, *Phys. Rev.* **D76** (2007) 075016, [arXiv:0706.3718 \[hep-ph\]](#).
- [30] B. Holdom *et al.*, [arXiv:0904.4698 \[hep-ph\]](#).
- [31] C. Amsler *et al.*, *Phys. Lett.* **B667** (2008) 1.
- [32] **CDF** Collaboration, R. Eusebi, [arXiv:0905.2548 \[hep-ex\]](#).
- [33] P. H. Frampton, P. Q. Hung, and M. Sher, *Phys. Rept.* **330** (2000) 263, [arXiv:hep-ph/9903387](#).

- [34] F. del Aguila, M. Perez-Victoria, and J. Santiago, *JHEP* **09** (2000) 011, [arXiv:hep-ph/0007316](#).
- [35] F. del Aguila, M. Perez-Victoria, and J. Santiago, *Phys. Lett.* **B492** (2000) 98–106, [arXiv:hep-ph/0007160](#).
- [36] J. A. Aguilar-Saavedra, [arXiv:0907.3155 \[hep-ph\]](#).
- [37] T. Appelquist, H.-C. Cheng, and B. A. Dobrescu, *Phys. Rev.* **D64** (2001) 035002, [arXiv:hep-ph/0012100](#).
- [38] N. Arkani-Hamed, A. G. Cohen, E. Katz, and A. E. Nelson, *JHEP* **07** (2002) 034, [arXiv:hep-ph/0206021](#).
- [39] G. Cynolter and E. Lendvai, *Eur. Phys. J.* **C58** (2008) 463–469, [arXiv:0804.4080 \[hep-ph\]](#).
- [40] R. S. Chivukula, B. A. Dobrescu, H. Georgi, and C. T. Hill, *Phys. Rev.* **D59** (1999) 075003, [arXiv:hep-ph/9809470](#).
- [41] G. Buchalla, G. Burdman, C. T. Hill, and D. Kominis, *Phys. Rev.* **D53** (1996) 5185–5200, [arXiv:hep-ph/9510376](#).
- [42] A. K. Leibovich and D. L. Rainwater, *Phys. Rev.* **D65** (2002) 055012, [arXiv:hep-ph/0110218](#).
- [43] S. Berge and W. Bernreuther, *Phys. Lett.* **B671** (2009) 470–476, [arXiv:0812.1910 \[hep-ph\]](#).
- [44] S. Berge, W. Bernreuther, and J. Ziethe, *Phys. Rev. Lett.* **100** (2008) 171605, [arXiv:0801.2297 \[hep-ph\]](#).